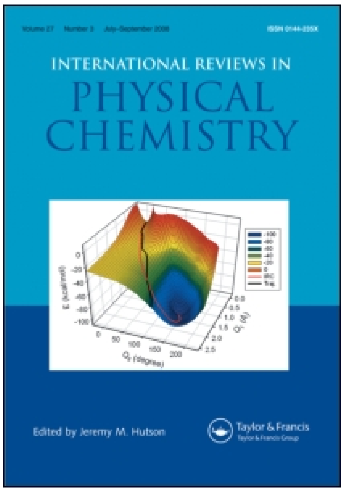

International Reviews in Physical Chemistry

Publication details, including instructions for authors and subscription information:
http://www.informaworld.com/smpp/title~content=t713724383

Theoretical study of the bonding in molecular transition-metal cations

Charles W. Bauschlicher Jr[a]; Stephen R. Langhoff[a]
[a] Ames Research Center, National Aeronautics and Space Administration, Moffett Field, California, USA

To cite this Article Bauschlicher Jr, Charles W. and Langhoff, Stephen R.(1990) 'Theoretical study of the bonding in molecular transition-metal cations', International Reviews in Physical Chemistry, 9: 2, 149 — 185

To link to this Article: DOI: 10.1080/01442359009353245

URL: http://dx.doi.org/10.1080/01442359009353245

INTERNATIONAL REVIEWS IN PHYSICAL CHEMISTRY, 1990, VOL. 9, NO. 2, 149–185

Theoretical study of the bonding in molecular transition-metal cations

by CHARLES W. BAUSCHLICHER, JR, and STEPHEN R. LANGHOFF
Ames Research Center, National Aeronautics and Space Administration,
Moffett Field, California 94035, U.S.A.

We review the bonding for both first- and second-row transition-metal positive ions with a variety of ligands. For singly charged ions we consider a range of interaction strengths from the weakly interacting noble gases to the covalently bonded dimethyls. We also consider several dications, since many of these systems are amenable to experimental study. The bonding, particularly for covalent systems, is found to arise generally from a mixture of the lowest atomic states. Polarization, sd and sp hybridization, and s-to-d and d-to-s promotion are various means of reducing the repulsion and enhancing the bonding. The relative importance of these effects depends on the separations between the lowest states of the metal ion. The loss of atomic d–d exchange energy in the molecule is also an important factor in determining the binding energies. The diversity of transition-metal bonding arises because the relative importance of these effects depends on the separation of the atomic states with different d occupancies. The calculations are able to explain the relative magnitudes of the first- and second-ligand binding energies for transition-metal ions bound to noble-gas, water, CO and CH_3 ligands.

1. Introduction

Considerable effort is being directed at understanding the bonding in transition-metal systems, because of their many uses as catalysts and in materials applications. While significant experimental progress has been made recently in both organometallic and surface science studies, a fundamental understanding of many aspects of the bonding is still lacking. For example, while perfect crystal faces are generally used in surface science experiments, catalysts consist of either imperfect crystals or small (very reactive) metal clusters. Also in organometallic studies it is frequently the average metal–ligand bond energy that is determined, while the critical step in homogeneous catalysis is often the breaking of the first bond. Thus there is great interest in understanding how the bonding changes with both the number of ligands and the number of metal atoms.

Experiments on neutral transition-metal systems, especially metal clusters, can be difficult, because of problems in selecting an individual system for study. However, these problems are considerably alleviated if the analysis is carried out for the corresponding positive ion. These ions are commonly produced by ionization of stable organometallic compounds followed by fragmentation, either by collision-induced dissociation (CID) or photodissociation (Buckner and Freiser 1988). Although the number of ions that can be produced this way is limited, binding energies are often obtained for the intermediate fragments. However, the recent development of laser ablation techniques coupled with a supersonic expansion source (Smalley 1985) has made it possible to generate metal clusters of arbitrary size, thus greatly increasing the number of ions that can be produced. The study of the reactivity of clusters as a function of size is expected to yield insight into the bonding within the clusters and between the clusters and adsorbates.

0144–235X/90 $3·00 © 1990 Taylor & Francis Ltd.

While cluster selection and isolation are easier for ions, their greater reactivity requires that they must be studied at relatively low densities. Although this complicates the spectroscopic characterization of these systems, improvements in sensitivity are making it possible to characterize vibrational frequencies and geometries. In addition, many other experimental techniques have been developed especially for ions. For example, the guided-ion beam approach (Armentrout and Georgiadis 1988) can be used to measure accurate binding energies, because ions can be accelerated and the added translational energy can drive an endothermic reaction. By determining the threshold for the reaction

$$M^+ + H_2 \rightarrow MH^+ + H,$$

the MH^+ binding energy can be determined. Unlike many of the organometallic techniques, this method determines individual bond energies. However, even reactions such as the one above can be difficult to analyse, as the excited metal ion states that are produced in the initial ionization process can be two orders of magnitude more reactive than the ground state, which can significantly lower the observed threshold. A related problem is that the internal temperature is not known. Nevertheless, more experimental data, especially for binding energies, are available for the transition-metal ions than for the corresponding neutrals. This provides part of the motivation for the theoretical studies presented in this review.

Ions can be trapped for long periods of time using ion cyclotron resonance (ICR) techniques. The longer containment time reduces problems with excited-state reactions. In addition ICR can be used to study the sequential products of a series of reactions or decompositions (Buckner and Freiser 1988). Binding energies of species are generally determined using CID or photodissociation techniques. For dications that dissociate to two cations, pair coincidence experiments can yield information about the potentials. If the molecule is vibrationally excited to its dissociation limit, the photon energy can be used to determine the barrier height, and the kinetic energy of the two ions gives the position of the potential well relative to the asymptotic limit. The existence of dications can also be confirmed using ion pair coincidence experiments by promoting the system to an excited dissociative state. As we show in section 3.7, many metastable dications are expected to exist with nearly infinite lifetimes. In principle, it should be possible to contain these systems with ICR techniques and to study them spectroscopically.

Experimental techniques are often applied to a whole series of transition-metal ions to obtain trends that give insight into the bonding. In many cases it has been possible to relate some of the variation in binding energy to atomic properties such as state splittings and loss of exchange energy (Armentrout and Georgiadis 1988). Attempts to relate the observations in the transition-metal ions with the better studied alkali or alkaline-earth ions have not been very successful. While experiments performed on beams of metal ions and atoms offer insight into the bonding of metals, they can be very difficult to interpret, and therefore *ab initio* calculations offer an attractive alternative for determining the origin of the variation between the different metals. Further, *ab initio* calculations have progressed to the point where they are providing quantitative results for transition-metal-containing systems (Langhoff and Bauschlicher 1988). Since the calculations are generally of nearly equal accuracy for all the metal ions, the calculations, in addition to explaining the origin of the observed trends, can be used to identify incorrect experimental values.

The plethora of experimental data for the positive ions has motivated considerable theoretical interest (for example Kunze and Harrison (1989), Schilling *et al.* (1987a, b) and Blomberg *et al.* (1987)). The experimental data for binding energies provide an excellent calibration for theory. Our laboratory has been very active in this area; we have studied transition metals bonded to a wide variety of ligands, and so we shall restrict the scope of this article to systems that we have studied and refer to other theoretical work only as it relates to our own. The calculations are presented in the order of the weakest interaction to the strongest. We first describe metal–noble-gas systems where the binding results primarily from a charge-induced dipole interaction. The calculations identify various mechanisms of reducing the metal–ligand repulsion. They also show that the bonding is not completely ionic, which explains why transition-metal ions bond more strongly than alkali metals to noble gases. We next consider the interaction of transition metals with one and two water molecules. The bonding in the metal–water systems is stronger, because of the charge–dipole interaction, but the metal–ligand repulsion is reduced by the same methods as in the noble-gas–transition-metal ions. However, the relative importance of the effects is changed by the fact that both the lone pair and the bonding orbitals of water interact with the metal d orbitals. The metal–CO interaction shows some dative metal-to-CO donation, so that the bonding contains some covalent character, in addition to the dominant electrostatic interactions. The transition-metal hydrides and methyls provide illustrations of covalent bonding. The monomethyls and dimethyls illustrate the change in the nature of the bonding with a second ligand; the change between the first and second covalently bound ligand is much larger than for the electrostatically bound ligands. The interaction of La^+ and La^{2+} with hydrocarbon ligands is used to compare and contrast covalent and electrostatic bonding. Our final example is the bonding in dications where strong chemical bonds are formed in spite of the Coulomb repulsion associated with two $+1$ charges.

2. Computational methods

To achieve accurate spectroscopic constants and binding energies for transition-metal systems, it is essential to account for electron correlation. In general we correlate the nd and $(n+1)$s electrons of the transition metals and all the valence electrons for the other species. In this work we use the self-consistent field (SCF) based modified coupled-pair functional (MCPF) method (Chong and Langhoff 1986, Ahlrichs *et al.* 1984) when the system is reasonably well described by a single configuration. Since the MCPF method accounts for some of the higher than double excitations, it is superior to a single-reference singles and doubles configuration-interaction (SDCI) treatment. In addition, the MCPF method is size consistent so that systems with different numbers of electrons can be treated with nearly equal accuracy. When the wavefunction is poorly described by a single-reference configuration, we use the complete active space SCF (CASSCF) based multireference configuration interaction (MRCI) approach. The CASSCF method allows the zeroth-order wavefunction to account for the near-degeneracies and bond correlation effects and more extensive correlation is added in the MRCI calculation (Siegbahn 1984). Higher excitations can then be included in an approximate manner using the multireference generalization of the Davidson correction or the averaged CPF (ACPF) method (Gdanitz and Ahlrichs 1988).

The one-particle basis sets used in the theoretical studies are at least of double-zeta-plus-polarization quality. For systems such as the noble-gas–transition-metal ions that are relatively weakly bound, we have determined the basis set superposition error

(BSSE) using the counterpoise method. Since the BSSE is always a small fraction of the binding energy and is cancelled by other effects such as basis set incompleteness, we generally ignore this effect. We frequently perform a basis set saturation study for one representative system to assess the limitations of the one-particle basis set. These basis set convergence tests show that the binding energies increase with increasing basis set saturation, so that in some cases, such as the monohydrides and monomethyls, we increase the computed binding energies slightly to account for basis set incompleteness.

For the second transition row, we use a relativistic effective core potential (RECP) that includes the mass–velocity and Darwin contributions (Cowan and Griffin 1976, Hay and Wadt 1985). The 4s and 4p semicore orbitals are not included in the RECP. This results in a node in the 5s orbital, which has been shown to be a necessity for a treatment including correlation (Rohlfing *et al.* 1986). The specific details about the basis set, correlation treatment and calibration studies can be found in the original publications.

One of our goals is to understand how the bonding in transition-metal systems varies for the different metal ions and ligands. We commonly use a Mulliken population analysis for this purpose. The Mulliken d populations are expected to be reliable, because the compact d orbitals should be relatively free from basis set artefacts. Because of the large overlap populations involving the valence s and p orbitals, these populations are not as reliable in an absolute sense. However, since we use similar metal basis sets, the trends among the metal ions for a given ligand are expected to be valid. These arguments are supported by density different plots and computed dipole moments, which are less subject to basis set artefacts. Therefore the populations can reveal important trends and give insight into the nature of the bonding.

3. Results and discussion

The bonding in transition-metal systems is significantly influenced by the mixing of the low-lying atomic states. This manifests itself as either sp or sd hybridization, or as promotion between the *n*d and $(n+1)$s shells, all of which can minimize repulsion or increase the strength of a covalent bond. Although the concepts of promotion and hybridization are straightforward and influence most chemical bonding, the hybridization of the metal s and d orbitals is less commonly encountered. Two different kinds of sd hybridization are illustrated by the logarithmic plot of the charge density of the Cr 4s and 3dσ orbitals given in figure 1, since the 4s orbital has a larger radial extent than the 3dσ orbital, it has a larger overlap with a ligand. The positive combination, a $4s+3d\sigma$ hybrid orbital, produces an orbital with an increased charge density along the z axis, while the minus combination $4s-3d\sigma$, decreases the charge density along the z axis, by building up charge in a torus about the metal in the x–y plane. When the s and d orbitals have equal occupancies, forming the hybrid orbitals with equal occupancy does not affect the repulsion, since this represents only a unitary transformation of equivalent orbitals. However, increasing the occupancy of the minus combination decreases the repulsion for a ligand approaching along the z axis. If the $4s-3d\sigma$ hybrid orbital contains more d than s character, moving charge into this hybrid orbital also involves mixing in $3d^{n+1}$ character into the wavefunction. As we show below, sd_σ hybridization is an important method of reducing the repulsion in electrostatic metal–ligand bonding. By reducing the metal–ligand repulsion for the non-bonding electrons in the $4s-3d\sigma$ hybrid orbital, the $4s+3d\sigma$ hybrid orbital forms a stronger covalent bond that if the bonding orbital contains only s character. For example, this is the principal bonding mechanism in the $^1\Sigma^+$ ground state of ScH (Bauschlicher and Walch

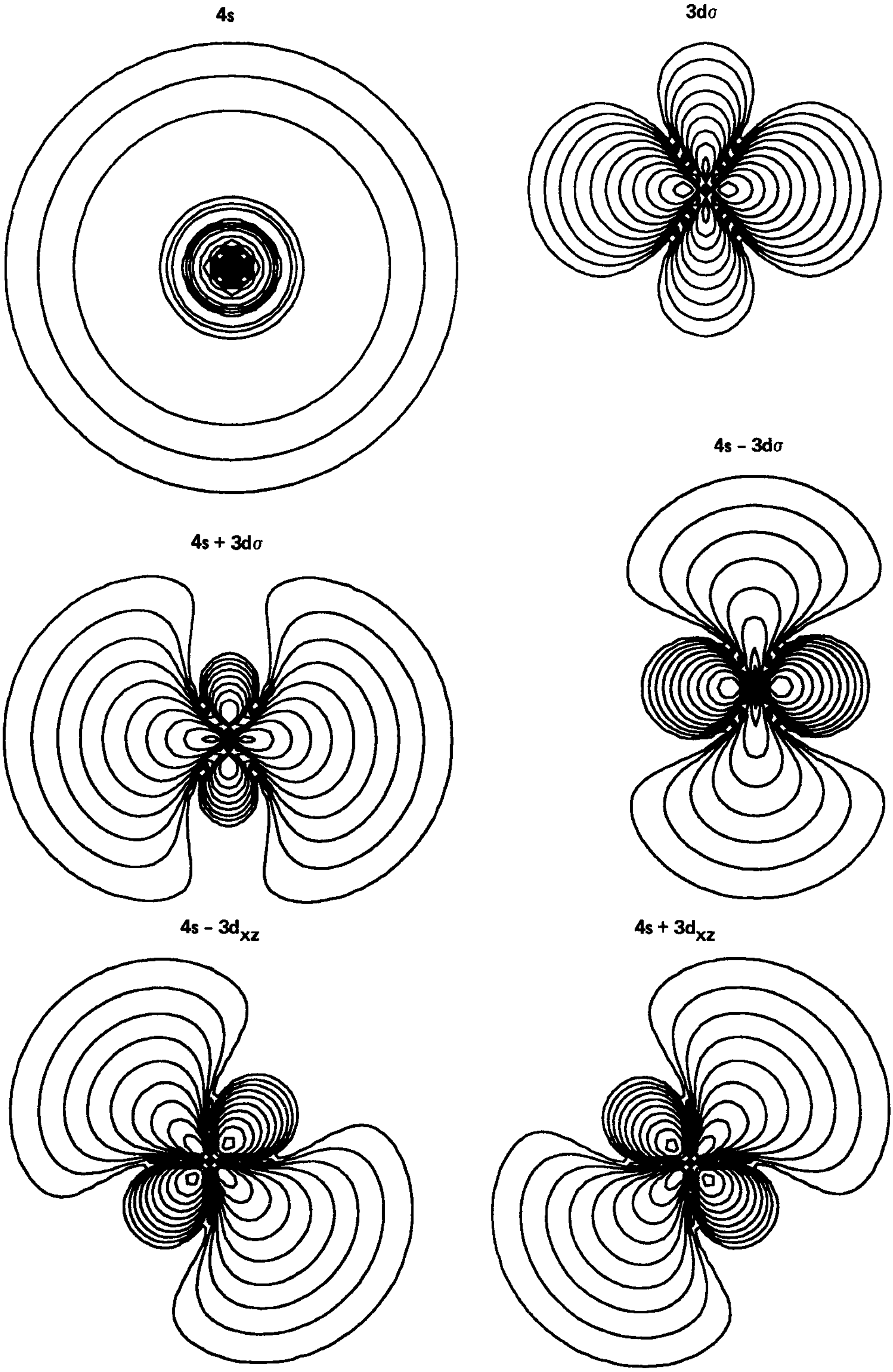

4s

3dσ

4s + 3dσ

4s - 3dσ

4s - $3d_{xz}$

4s + $3d_{xz}$

Figure 1. A plot of the 4s and 3dσ orbitals of the Cr atom, and the $4s3d_\sigma$ and $4s3d_{xz}$ hybrid orbitals.

1982). Also shown in figure 1 are the two equivalent hybrid orbitals with maximum charge density at 90° angles that result from hybridization of the 4s and $3d_{xz}$ orbitals. This sd hybridization is ideal for forming two covalent bonds and is the reason that all the $M(CH_3)_2^+$ molecules discussed below have C–M–C angles near 90°.

3.1. *Bare transition-metal ions*

Given that several atomic states typically contribute to the bonding, the calculations must be able to describe the separation between the low-lying $d^{n-1}s^2$, d^ns^1 or d^{n+1} atomic states of the ion to be able to account correctly for the mixing that occurs in the molecular system. The calculated separations between the two lowest states for the first- and second-row transition-metal ions are compared with experiment in table 1. The average error in the separations between the lowest two atomic states is not strongly dependent on the f-polarization set, changing by only 0·01 eV when a 3f set replaces a 1f set (Bauschlicher *et al.* 1989b). Using the 1f polarization set, the average error in the separations for the second-row ions is only 0·17 eV, with most of this error occurring for the Mo, Tc and Ag separations. For the first-row transition-metal ions, the average error of 0·15 eV in the non-relativistic calculations is increased to 0·37 eV when a correction is added for the mass–velocity and Darwin relativistic corrections using first-order perturbation theory. Since the molecular wavefunctions mix in some neutral metal character, it is also important to be able to describe the d^ns^2, $d^{n+1}s^1$ and d^{n+2} separations of the neutrals. The average errors in these separations are

Table 1. Atomic excitation energies computed at the MCPF level for the first- and second-row transition-metal positive ions. The relativistic values for the first-row transition-metal ions include a perturbation theory estimate of the Darwin and mass–velocity terms. Experimental results are the *j*-averaged values given by Moore (1949).

			ΔE (eV)		
Ion	Lower state	Upper state	Non-relativistic	Relativistic	Experiment
		First-row transition-metal ions			
Sc^+	$3d^14s^1$ (^3D)	$3d^2$ (^3F)	0·75	0·91	0·60
Ti^+	$3d^24s^1$ (^4F)	$3d^3$ (^4F)	0·20	0·39	0·10
V^+	$3d^4$ (^5D)	$3d^34s^1$ (^5F)	0·31	0·07	0·33
Cr^+	$3d^5$ (^6S)	$3d^44s^1$ (^6D)	1·70	1·41	1·52
Mn^+	$3d^54s^1$ (^7S)	$3d^6$ (^5D)	2·13	2·43	1·81
Fe^+	$3d^64s^1$ (^6D)	$3d^7$ (^4F)	0·40	0·76	0·25
Co^+	$3d^8$ (^3F)	$3d^74s^1$ (^5F)	0·30	−0·10	0·43
Ni^+	$3d^9$ (^2D)	$3d^84s^1$ (^4F)	0·98	0·54	1·08
Cu^+	$3d^{10}$ (^1S)	$3d^94s^1$ (^3D)	3·02	2·53	2·81
		Second-row transition-metal ions			
Y^+	$5s^2$ (^1S)	$4d^15s^1$ (^3D)		0·23	0·15
Zr^+	$4d^25s^1$ (^4F)	$4d^3$ (^4F)		0·25	0·32
Nb^+	$4d^4$ (^5D)	$4d^35s^1$ (^5F)		0·45	0·33
Mo^+	$4d^5$ (^6S)	$4d^45s^1$ (^6D)		1·95	1·59
Tc^+	$4d^55s^1$ (^7S)	$4d^6$ (^5D)		0·90	0·52
Ru^+	$4d^7$ (^4F)	$4d^65s^1$ (^6D)		1·04	1·09
Rh^+	$4d^8$ (^3F)	$4d^75s^1$ (^5F)		2·15	2·13
Pd^+	$4d^9$ (^2D)	$4d^85s^1$ (^4F)		3·22	3·19
Ag^+	$4d^{10}$ (^1S)	$4d^95s^1$ (^3D)		5·47	5·04

comparable with those for the ions. The larger errors for the separations that include relativistic effects can be explained by the fact that the MCPF calculations describe the $d^ns^1(d^ns^2)$ occupancies, which have less d–d correlation, better than the $d^{n+1}(d^{n+1}s^1)$ occupancies. Since there is more relativistic energy associated with the s than with the d electrons, relativistic effects add an additional bias in favour of the $d^ns^1(d^ns^2)$ occupancies, and therefore the inclusion of relativistic effects increases the error for most of the ions (and atoms). The calculated errors in the atomic splittings may introduce some errors in the description of the molecular systems; this error is expected to be small and is discussed in more detail below for selected systems.

3.2. *Metal–noble-gas systems*

The dominant interaction of a metal ion with a noble-gas atom arises from charge-induced polarization of the noble-gas atom. If this were the only important interaction, then the bond strength of a diatomic molecule, whether it involved a transition-metal or alkali atom, would be related to the size of the ion and noble-gas atom and the polarizability of the noble-gas atom. The size of the atoms determines the internuclear separation where the Pauli repulsion balances the attractive forces. In the analysis of their resonant photodissociation data, Lessen and Brucat (1988) used a potential of the form

$$U(r)=ar^{-12}-\tfrac{1}{2}q\alpha r^{-4},$$

where r is the metal-ion–noble-gas atom internuclear separation, α is the polarizability of the noble gas atom, q is the charge on the metal ion and a is an adjustable parameter used to describe the repulsive forces. Thus, for a given noble-gas atom, the interaction energy should depend only on the size of the metal ion. However, the experimental results indicate that the transition-metal ions are more strongly bound than the alkali ions. It is important to understand the origin of this difference as the energy required to detach, for example, an Ar atom from an M_nAr^+ cluster is expected to be used as a probe for the cluster temperature. This is accomplished by finding the threshold for the process

$$M_n^+Ar\xrightarrow{h\nu}M_n^+ + Ar;$$

then the binding energy is given as the energy shift from the bare M_n^+ cluster absorption, assuming that Ar only weakly perturbs the metal cluster ion. As internal energy is added to the cluster, the energy shift is reduced, thereby providing a probe of the cluster temperature. For a diatomic molecule, the internal temperature depends on the vibrational distribution and hence is directly related to the reduction in the energy required to dissociate the system. However, in a larger cluster the analysis is complicated by the fact that not all the internal energy may be used to reduce the energy required to remove the Ar. Nevertheless, considering that little is known about the temperature of the clusters, these experiments may supply valuable information.

We have studied (Bauschlicher and Langhoff 1989a, Bauschlicher *et al.* 1989a) a number of the metal–noble-gas diatomic ions, since these are straightforward from both an experimental and a theoretical point of view. The results of our theoretical study are compared with experiment in table 2. We report the dissociation energy D_0, the bond length r_e, the vibrational frequency ω_e and the excitation energy T_e. To facilitate the comparison of the bonding arising from different metal asymptotes, we report the D_0 value of each electronic state relative to the atomic asymptote from which it is derived. Experimental data for the transition-metal–noble gas ions are obtained

Table 2. Spectroscopic constants for selected metal–noble-gas ions.

State	r_e (units of a_0)	D_0 (eV)	ω_e (cm^{-1})	T_e (cm^{-1})
	Theoretical			
VAr^+ $^5\Sigma^+(3d\pi^2 3d\delta^2)$	5·015	0·291	143	
FeAr^+ $^6\Delta(3d\sigma^1 3d\pi^2 3d\delta^3 4s^1)$	5·422	0·140	86	0
FeAr^+ $^4\Delta(3d\sigma^2 3d\pi^2 3d\delta^3)$	4·688	0·297	172	1686
FeAr^+ $^4\Phi(3d\sigma^1 3d\pi^3 3d\delta^3)$	4·748	0·331	154	2861
CoAr^+ $^3\Delta(3d\sigma^1 3d\pi^4 3d\delta^3)$	4·597	0·392	177	0
CoAr^+ $^3\Phi(3d\sigma^2 3d\pi^3 3d\delta^3)$	4·613	0·131	165	2109
CoAr^+ $^3\Pi(3d\sigma^1 3d\pi^3 3d\delta^4)$	4·665	0·348	173	2843
NiAr^+ $^2\Sigma^+(3d\sigma^1 3d\pi^4 3d\delta^4)$	4·488	0·450	210	0
NiAr^+ $^2\Delta(3d\sigma^2 3d\pi^4 3d\delta^3)$	4·510	0·342	161	909
NiAr^+ $^2\Pi(3d\sigma^2 3d\pi^3 3d\delta^4)$	4·588	0·338	165	938
CuHe^+ $^1\Sigma^+$	3·808	0·068	228	
CuAr^+ $^1\Sigma^+$[a]	4·486	0·379	194	
CuKr^+ $^1\Sigma^+$	4·658	0·571	153	
LiAr^+ $^1\Sigma^+$	4·578	0·238	245	
LiKr^+ $^1\Sigma^+$	4·844	0·309	256	
NaAr^+ $^1\Sigma^+$	5·438	0·120	112	
KAr^+ $^1\Sigma^+$	6·472	0·061	66	
MgAr^+ $^2\Sigma^+$	5·444	0·127	98	

State	r_e (units of a_0)	D_0 (eV)
	Experimental	
VAr^+		0·369[b]
CoAr^+		0·508[c]
NiAr^+		0·550[d]
LiAr^+	4·60[g], 4·55[h]	0·550[e], 0·303 ± 0·004[f], 0·276[g], 0·318[h]
LiKr^+		0·710[e]
NaAr^+	6·50[i]	0·211[e], 0·119[i]
KAr^+	6·59[i], 6·28[j], 5·7[k], 5·4[l]	0·119[e], 0·064[i], 0·085[j], 0·12[k], 0·14[l]

[a] Using a larger Ar basis, r_e, D_0 and ω_e are $4{\cdot}487a_0$, 0·405 eV and 193 cm^{-1}.
[b] Lessen and Brucat (1989b).
[c] Lessen and Brucat (1989a).
[d] Lessen and Brucat (1988).
[e] Takebe (1983), mobility data.
[f] Böttner *et al.* (1975), scattering data.
[g] Gatland (1981), mobility data.
[h] Polak-Dingels *et al.* (1982), scattering data.
[i] Powers and Cross (1973), scattering data.
[j] Lamm *et al.* (1981), mobility data.
[k] Schamp and Mason (1958), mobility data.
[l] Skullerud (1973), mobility data.

from photodetachment experiments, while those for the alkali–noble-gas ions are based on either scattering or ion mobility data. The latter values are subject to larger errors but, unlike the photodetachment experiments, give the bond length directly.

The theoretical D_0 values for VAr^+, CoAr^+ and NiAr^+ are all about 0·1 eV less than experiment (Lessen and Brucat 1988, 1989a). Since the BSSEs are negligible, this difference must be ascribed either to limitations of the one-particle basis sets or to the MCPF treatment of electron correlation. Despite these limitations, theory provides a balanced treatment for these systems. For $NiAr^+$ we considered the $^2\Sigma^+$, $^2\Pi$ and $^2\Delta$ states derived from the Ni^+ $^2D(3d^9)$ ground state. The occupancies of these states are similar, except for the orientation of the 3d hole. The $^2\Sigma^+$ state is the most stable since repulsion is minimized by having only one electron in the 3dσ orbital, which has the largest overlap with the Ar. The $^1\Sigma^+$ state of $CuAr^+$ is more strongly bound than either the $^2\Delta$ or the $^2\Pi$ states of $NiAr^+$, because Cu^+ has a smaller radial extent than Ni^+. However, the fact that the $^2\Sigma^+$ state of $NiAr^+$ is more stable than the $^1\Sigma^+$ state of $CuAr^+$ shows the importance of localizing the hole in the 3dσ orbital to reduce the repulsion. This effect is important in determining the ground state of $CoAr^+$ and VAr^+; $CoAr^+$ has a $^3\Delta$ ground state with a hole in the 3dσ orbital and VAr^+ has a $^5\Sigma^+$ ground state, which is derived from the V^+ $3d^4$ occupancy that has the 3dσ orbital empty.

Unlike the ground states of VAr^+, $CoAr^+$, $NiAr^+$ and $CuAr^+$, all of which are derived from the $3d^{n+1}$ occupation, the ground state of $FeAr^+$ is derived from the $3d^n4s^1$ occupancy of Fe^+. Owing to the larger radial extent of the 4s orbital, the r_e value of the $^6\Delta$ ground state of $FeAr^+$ is considerably larger than for states derived from the $3d^{n+1}$ occupancy. Since the attractive potential goes like r^{-4}, the longer bond length leads to much weaker bonding. If we consider instead the $^4\Phi$ and $^4\Delta$ states derived from the $3d^7$ asymptote of Fe^+, the bond energy is similar to the other systems derived from the $3d^{n+1}$ occupancy. However, these remain excited states of $FeAr^+$, because the relatively weak interaction does not compensate for the promotion energy.

Comparable calculations on selected alkali-ion–noble-gas diatomics indicate that they are significantly less strongly bound than the transition-metal–noble-gas ions. This observation is inconsistent with purely electrostatic arguments, considering that the alkali ions are smaller in radial extent. In fact, on the basis of these electrostatic arguments, Lessen and Brucat (1989a, b) suggested that even the larger experimental D_0 values for the alkali–noble-gas systems determined from ion mobility data might be too small. However, all theoretical calculations (Bauschlicher *et al.* 1989a, Olson and Liu 1979, Ahlrichs *et al.* 1988) indicate that the alkali-ion–noble-gas binding energies are considerably less than the larger values derived from ion mobility data. Based on the fact that the SCF and MCPF levels yield the same binding energy for the alkali ions but that the MCPF D_0 is twice the SCF value for the transition-metal ions, it was suggested that the bonding in the alkali systems is completely electrostatic M^+Ar, while there is some M^0Ar^+ mixing into the transition-metal systems, because of the larger ionization potential (IP) of the transition-metal atoms. This model was tested using the series $CuHe^+$, $CuAr^+$ and $CuKr^+$. The binding energies at the SCF level, $CuKr^+ > CuAr^+ > CuHe^+$, reflect the noble-gas atom polarizability. The effect of correlation on D_0 follows the same trend, as a result of the decrease in noble-gas atom IP, which allows more Cu^0L^+ to mix in. Further, combining the computed increase in the CuKr binding energy relative to CuAr with the experimentally observed increase for V and Co, we find that the effect is Cu > Co > V, which follows the IP of the metals. Finally we note that $MgAr^+$ also shows an increase in binding when correlation is added. Thus the correlation effect that introduces M^0L^+ character into the wavefunction is present for a system where correlation improves the description of the metal IP even though it does not have occupied 3d orbitals. Therefore we conclude that the calculations definitively show that an admixture of M^0L^+ is an important component in the transition-metal systems.

In summary, calculations for metal ions interacting with one noble-gas atom have shown that localizing the 3d hole dictates the ordering of the states, as it lowers the Pauli repulsion and decreases the shielding of the nucleus. Those ions with the 4s orbital occupied are more weakly bound, because the larger radial extent of the 4s orbital results in longer bond lengths and therefore a reduced electrostatic interaction. Since the bonding is relatively weak, promotion of the s orbital into the d shell will occur only when the $d^ns^1-d^{n+1}$ separation is quite small. The calculations have also shown that transition-metal ions are bound more strongly to noble-gas atoms than are alkali atoms, because the larger transition-metal IP allows some M^0L^+ character to mix into the wavefunction. This effect is significantly enhanced at the correlated level.

The bonding of a second noble-gas atom to a metal ion is also electrostatic in origin. Therefore the second-ligand binding energy is expected to be comparable with or slightly less than the first, because of ligand–ligand repulsion and charge donation to the metal ion by the first ligand, which will reduce the effective charge on the metal ion. While this trend in binding energies has been observed for the alkali ions interacting with water molecules, experiments have found the second water ligand to be more strongly bound than the first for some transition-metal ions (Magnera *et al.* 1989, Marinelli and Squires 1989). We consider the bonding of water molecules to transition metals in the next section, after we first consider the binding of a second noble-gas atom to many of the metal ions studied above.

Spectroscopic constants and binding energies for selected metal ions bonded to one and two noble-gas atoms are compared in table 3. The second noble-gas binding energies are found to be greater than or equal to the first (Bauschlicher *et al.* 1990). Although differences of less than 0·01 eV may not be significant owing to the neglect of BSSE and relativistic effects, the trends should be meaningful. Therefore, within the limitations of the calculations, the binding energy for the second Ar atom is equal to the first for Li^+, Na^+, Mg^+ and V^+. All ML_2^+ molecules, with the exception of $MgAr_2^+$, have linear ground states. The reason that $MgAr_2^+$ is strongly bent (bond angle of 82·5°) is evident from figure 2, where we plot the open-shell 3s-like orbital. When one Ar atom approaches Mg^+, the 3s electron polarizes away to reduce the repulsion and to enhance the electrostatic interaction. However, when two Ar atoms approach Mg^+ from opposite sides, the 3s electron cannot polarize, and the second Ar is bound by 0·046 eV less than the first. However, if both Ar atoms approach Mg^+ from the same side, polarization of the 3s electron reduces the repulsion with both Ar atoms simultaneously (see figure 2). At the optimal geometry, the binding energy of the second Ar ligand is essentially the same as the first.

It is very enlightening to compare the results for $FeAr^+$ and $FeAr_2^+$ in table 3. As mentioned previously, the ground state of $FeAr^+$ is the weakly bound $^6\Delta$ state arising from the $3d^64s^1$ state of Fe^+. The addition of a second Ar ligand to the $^6\Delta$ state of $FeAr^+$ results in a bent $FeAr_2^+$ sextet state ($^6A_1$) with a small Ar–Fe–Ar angle. Although bending increases the binding energy by 0·043 eV, the second Ar is still bound by less than the first. This state cannot reduce the repulsion by sd hybridization, because the 4s electron is high-spin coupled to the 3d shell. However, the repulsion in $FeAr_2^+$ can also be reduced by promoting the 4s electron into the compact 3d orbital. For $FeAr^+$ this produces a $^4\Delta$ excited state, because the promotion energy is not compensated for by the enhancement in the bonding. However, $FeAr_2^+$ has a $^4\Delta_g$ ground state that arises from the $3d^7$ asymptote of Fe^+, because the promotion energy is now amortized over two bonds. This results in a larger binding energy for the second Ar atom.

The second binding energy is also greater than the first for Co^+, Ni^+ and Cu^+, even though in these systems there is no change in the metal ion occupancy when the second Ar ligand bonds. While this increase is small, the calculations should be sufficiently

Table 3. Spectroscopic constants for selected metal–noble-gas ions.

	$ML^{+\,a}$			ML_2^+				
System state	r_e (units of a_0)	D_e (eV)	T_e (cm^{-1})	State	r_e (units of a_0)	D_e (eV)	T_e (cm^{-1})	ΔD_e ^{b}
VAr^+ $^5\Sigma^+(3d\pi^2 3d\delta^2)$	5·015	0·299	—	$^5\Sigma_g^+$	5·029	0·596	—	−0·002
$FeAr^+$ $^6\Delta(3d\sigma^1 3d\pi^2 3d\delta^3 4s^1)$	5·422	0·145	0	$^6\Delta_g$	5·861	0·231	1090	−0·059
				$^6A_1$	5·572^c	0·274	742	−0·016
$FeAr^+$ $^4\Delta(3d\sigma^2 3d\pi^2 3d\delta^3)$	4·688	0·308	1686	$^4\Delta_g$	4·576	0·739	0	+0·123
		(−0·075)^d				(0·366)^d		(+0·076)^e
$CoAr^+$ $^3\Delta(3d\sigma^1 3d\pi^4 3d\delta^3)$	4·597	0·392	0	$^3\Delta_g$	4·551	0·827	—	+0·043
$NiAr^+$ $^2\Sigma^+(3d\sigma^1 3d\pi^4 3d\delta^4)$	4·488	0·464	0	$^2\Sigma_g^+$	4·463	0·942	0	+0·014
$NiAr^+$ $^2\Delta(3d\sigma^2 3d\pi^4 3d\delta^3)$	4·510	0·351	909	$^2\Delta_g$	4·416	0·844	932	+0·142
$NiAr^+$ $^2\Pi(3d\sigma^2 3d\pi^3 3d\delta^4)$	4·588	0·348	938	$^2\Pi_u$	4·495	0·798	1304	+0·102
$CuHe^+$ $^1\Sigma^+$	3·808	0·082	—	$^1\Sigma_g^+$	3·689	0·178	—	+0·014
$CuAr^+$ $^1\Sigma^+$	4·486	0·392	—	$^1\Sigma_g^+$	4·418	0·850	—	+0·066
$CuKr^+$ $^1\Sigma^+$	4·658	0·581	—	$^1\Sigma_g^+$	4·583	1·212	—	+0·050
$LiAr^+$ $^1\Sigma^+$	4·578	0·253	—	$^1\Sigma_g^+$	4·588	0·510	—	+0·004
$NaAr^+$ $^1\Sigma^+$	5·438	0·127	—	$^1\Sigma_g^+$	5·434	0·264	—	+0·010
$MgAr^+$ $^2\Sigma^+$	5·444	0·133	—	$^2\Sigma_g^+$	5·861	0·220	—	−0·046
				$^2A_1$	5·559^f	0·269	—	+0·003

[a] Taken from Bauschlicher and Langhoff (1989a) and Bauschlicher *et al.* (1989a).

[b] The change in D_e between the first and second noble-gas atom; that is $D_e(ML_2^+) - 2D_e(ML^+)$.

[c] The bond angle is 80·8°.

[d] The value in parentheses is relative to the ground state asymptote $^6D(3d^6 4s^1)$, whereas the other value is with respect to Fe^+ $^4F(3d^7)$.

[e] The value is computed relative to the $^6\Delta$ ground state of $FeAr^+$.

[f] The bond angle is 82·5°.

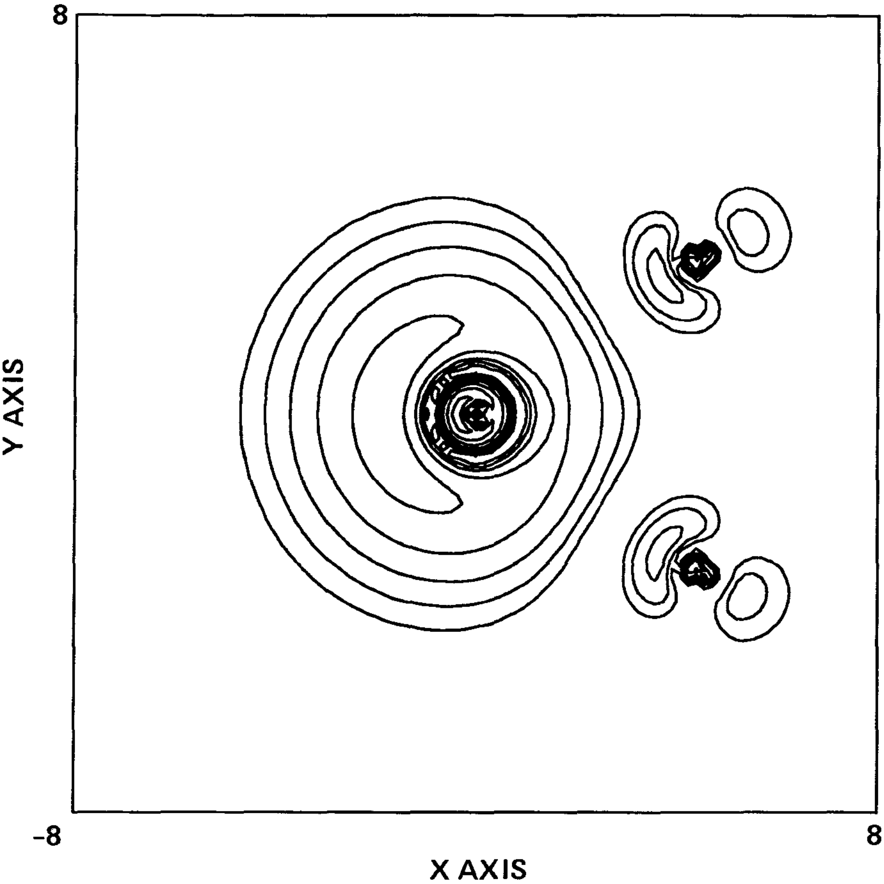

Figure 2. A contour plot of the open-shell SCF orbital for $MgAr_2^+$ showing the polarization of the Mg 3s electron away from the approaching Ar atoms. The Mg^+ ion is at the origin.

accurate to predict this trend correctly. The larger binding energy for the second Ar ligand probably arises from sd hybridization, which reduces the metal–Ar repulsion. It has been shown that the positive combination of the 4s and 3dσ orbitals increases the charge density along the bond axis, while the negative combination decreases it. Thus all these systems are linear because sd hybridization minimizes the repulsion along the bond axis. Electron correlation increases the importance of sd hybridization, and we find that the second Ar binding energy is less than the first for Cu^+ at the SCF level, but more at the MCPF level. Although sd hybridization probably also occurs with one Ar ligand, it is more important for two since they share the cost of the hybridization. For V^+, the first- and second-Ar atom binding energies are comparable, since no sd hybridization is possible as the 3dσ orbital is unoccupied. The first and second Ar binding energies are also comparable for Li^+ and Na^+ where there are no valence electrons to hybridize or polarize.

In summary, calculations for metal ions bound to one and two noble-gas atoms show that the hybridization or promotion can become more important when two noble-gas atoms are present, since the cost of changing the configuration of the metal ion is now amortized over two noble-gas atoms. The calculations also show that there is competition between sd hybridization (or promotion) and 4s–4p polarization. Thus whether the system is linear or bent depends on the relative energies of the $3d^n4s^1$ and $3d^{n+1}$ occupancies. Hence the diversity of the bonding in transition-metal systems manifests itself even for the relatively weak transition-metal–noble-gas interaction.

3.3. *Transition-metal–water systems*

The experimental data for the interaction of one or more water molecules with a transition metal indicate that, like the noble-gas ions, water interacts quite differently with transition-metal ions than with alkali ions (Magnera *et al.* 1989, Marinelli and Squires 1989). Most notably, the second water ligand is more strongly bound than the first for some ions. Based on the theoretical calculations for the transition-metal–noble-gas systems, the enhancement in the second-ligand binding energy must come from hybridization or promotion on the metal, which becomes more favourable when the cost of changing the state of the metal ion is shared by two water ligands (Rosi and Bauschlicher 1989).

Calculations for MH_2O^+ show that the planar system is the most stable, but that bending the H atoms out of the plane requires very little energy. SCF calculations for $Cu(H_2O)_2^+$ show that the most stable configuration is the staggered D_{2d} configuration with a linear O–Cu–O geometry. However, since the planar D_{2h} configuration is only slightly higher in energy, this geometry was selected to simplify the calculations. Thus, we consider bending the system with the constraint of C_{2v} symmetry, that is we bend the O–M–O angle but keep the metal ion and each water ligand in a plane. For the monowater and planar diwater systems, the metal 3d orbitals were found to have local linear symmetry and therefore we denote the d orbitals in this manner.

The interaction of a metal ion with H_2O is much stronger than with noble-gas atoms, because the interaction now has a charge-dipole contribution to the bonding as well as the terms discussed for the metal–noble-gas interaction. In addition, the overlap of a water ligand with the metal ion is more complex than for the spherical Ar atom. Of the H_2O orbitals, the σ (a_1) lone-pair orbital has the largest overlap with the 4s and $3d\sigma$ metal orbitals. The H_2O $\pi(b_2)$ lone pair and H–O bonding (b_1) orbital both overlap with the $3d\pi$ orbitals. The π lone-pair orbital has a larger overlap, because the O–H bond is bent away from the metal atom. Both of these overlaps are smaller than that in the σ space. The $3d\delta$ metal orbitals have very small overlaps with the water ligands. Thus the order of repulsion for the metal 3d orbitals with water is

$$3d\sigma(a_1) > 3d\pi(b_2) > 3d\pi(b_1) > 3d\delta(a_1) \approx 3d\delta(a_2).$$

Thus one important factor determining the binding energy will be the orientation of the 3d holes as a method of minimizing the repulsion. As noted for $FeAr_n^+$, there is competition between promotion, hybridization and bending in reducing the repulsion. Owing to the stronger bonding in the water systems, the relative importance of these effects can vary between the different metal ions and between the noble-gas and water ligands.

The computed and experimental results for transition-metal–water systems are summarized in tables 4 and 5. We consider selected metal ions to illustrate the differences and similarities in the bonding to water and noble-gas ligands. The bonding in $Sc(H_2O)^+$ is dominated by the lowest atomic asymptote of Sc^+, $^3D(3d^14s^1)$, because the first excited state of Sc^+, $^3F(3d^2)$, lies 13·8 kcal mol^{-1} higher in energy. Thus the

Table 4. MCPF bond distances, populations and binding energies for the ground states of the $M(H_2O)_n^+$ ions.

	Sc	Ti	V	Cr	Mn	Fe	Co	Ni	Cu
				MH_2O^+					
State	$^3A_1$	$^4B_1$	$^5A_1$	$^6A_1$	$^7A_1$	$^6A_1$	$^3B_2$	$^2A_1$	$^1A_1$
r(M–O) (units of a_0)	4·259	4·034	3·951	4·055	4·158	3·996	3·764	3·733	3·728
$D_e(M^+–H_2O)$ (kcal mol^{-1})	36·2	39·2	36·4	31·8	30·2	35·4	39·9	42·8	39·0
3d population	1·16	2·24	3·32	4·90	5·01	6·02	7·84	8·97	9·89
4s population	0·91	0·84	0·75	0·15	0·98	0·98	0·21	0·10	0·16
4p population	0·07	0·07	0·07	0·05	0·12	0·15	0·07	0·08	0·08
				$M(H_2O)_2^+$					
State	$^3B_{1g}$	$^4B_{2g}$	$^5B_{3g}$	^6A_g	$^7A_1$†	$^4B_{1g}$	$^3B_{3g}$	$^2B_{3g}$	^1A_g
r(M–O) (units of a_0)	4·296	4·077	3·962	3·975	4·245	3·762	3·703	3·656	3·668
D_e $(MH_2O^+–H_2O)$ (kcal mol^{-1})	31·6	35·2	39·3	33·9	22·9	38·4	40·7	39·6	39·2
3d population	1·35	2·43	3·63	4·74	5·03	6·50	7·66	8·73	9·76
4s population	0·80	0·73	0·54	0·41	0·96	0·66	0·51	0·44	0·42
4p population	0·09	0·09	0·09	0·08	0·21	0·12	0·13	0·14	0·13

† Bent geometry with an O–Mn–O angle of 93·8°.

Table 5. D_0 values for the $M(H_2O)_n^+$ ions.

	Sc	Ti	V	Cr	Mn	Fe	Co	Ni	Cu
			Present work†						
$D_0(M^+–H_2O)$ (kcal mol^{-1})	34·5	37·5	34·7	30·1	28·5	33·7	38·2	41·1	37·3
$D_0(MH_2O^+–H_2O)$ (kcal mol^{-1})	30·2	33·8	37·9	32·5	21·5	37·0	39·3	38·2	37·8
Δ (kcal mol^{-1})	−4·3	−3·7	+3·2	+2·4	−7·0	+3·3	+1·1	−2·9	+0·5
			Magnera *et al.* (1989)						
$D_0(M^+–H_2O)$ (kcal mol^{-1})	31·4	38·0	36·2	29·0	32·5	28·8	37·1	36·5	35·0
$D_0(MH_2O^+–H_2O)$ (kcal mol^{-1})						38·0	45·0	38·0	39·0
Δ (kcal mol^{-1})						+9·2	+7·9	+1·5	+4·0
			Marinelli and Squires (1989)						
$D_0(M^+–H_2O)$ (kcal mol^{-1})			35·1	21·9	26·5	32·8	40·1	39·7	
$D_0(MH_2O^+–H_2O)$ (kcal mol^{-1})			35·5	29·5	17·8	40·8	41·9	40·6	
Δ (kcal mol^{-1})			+0·4	+7·6	−8·7	+8·0	+1·8	+0·9	

† The SCF level zero point corrections from $Cu(H_2O)_n^+$ are used for all systems.

order of the low-lying excited states is determined by the orientational preference of the 3d electron, which is

$$^3A_1(3d\delta_{x^2-y^2}) < {}^3A_1(3d\delta_{xy}) < {}^3B_1(3d\pi_{xz}) < {}^3B_2(3d\pi_{yz}) < (2)^3A_1(3d\sigma)$$

with relative energies 0, 1·8, 5·3, 9·9 and more than 9·9 kcal mol^{-1}. As a consequence of the increased Pauli repulsion from occupying the 3dσ orbital, the $(2)^3A_1$ state lies above the $^3B_2$ state. The $^1A_1$ state of $Sc(H_2O)^+$, which is derived principally from the $^1D(3d^14s^1)$ state, is 8·8 kcal mol^{-1} above the ground state. This state has the 3dσ orbital singly occupied and therefore has the same occupation as the $(2)^3A_1(3d\sigma)$ state. Relative to the triplet state, the singlet must pay the atomic promotion energy, but the metal–water repulsion is reduced by sd hybridization, since the repulsion is decreased by moving charge density from the 4s + 3dσ orbital into the 4s − 3dσ orbital. In spite of the larger promotion energy for the $^1A_1$ state, this hybridization substantially reduces the repulsion, resulting in a larger binding energy for the $^1A_1$ state than for the $^3B_2$ state. The second water ligand is less strongly bound than the first, since the charge-transfer contribution to the binding causes the second water ligand to see a smaller positive charge. Also, for two water ligands any sp hybridization is lost since the water ligands approach from opposite sides of the ion. It is interesting to note that more $3d^2$ mixes into the wavefunction for $Sc(H_2O)_2^+$, since the promotion energy is amortized over two water ligands. Although promotion into the more compact 3d orbital reduces the repulsion, this reduction is not very large for Sc^+ owing to the more similar radial extents of the 3d and 4s orbitals on the left-hand side of the row. Thus sd promotion does *not* lead to a larger binding energy for the second water ligand. However, the sd hybridization is sufficiently important that the O–Sc–O bond angle remains at 180°.

The nature of the bonding between Mn^+ and H_2O is dictated by the very large $3d^n4s^1$–$3d^{n+1}$ atomic separation in Mn^+. The bonding in MnH_2O^+ is derived principally from the Mn^+ $3d^54s^1$ atomic state, since the $3d^6$ state of Mn^+ lies 43 kcal mol^{-1} higher. The large radial extent of the Mn^+ 4s orbital leads to a large repulsion with the H_2O ligand. This repulsion is reduced by sp hybridization, which allows polarization away from the water ligand. The importance of this polarization for the first water ligand is evident from the very small (14·4 kcal mol^{-1}) second-water-ligand binding energy if $Mn(H_2O)_2^+$ is constrained to be linear (i.e. a ^7A_g state). Since for the linear configuration 4s–4p polarization is no longer possible, it becomes energetically favourable to bend $Mn(H_2O)_2^+$ or to promote the Mn^+ to the $^5D(3d^6)$ atomic state. However, because of the very large promotion energy, the ^5A_g state, which is derived from a mixture of the $^5S(3d^54s^1)$ and $^5D(3d^6)$ states of the metal ion, is only slightly more bound than the linear ^7A_g state. Thus bending proves to be energetically optimal and the ground state of $Mn(H_2O)_2^+$ is the bent $^7A_1$ state. However, the binding energy of the second water ligand (22·9 kcal mol^{-1}) is still smaller than that of the first.

The bonding between Fe^+ and H_2O has considerable similarity to that between Mn^+ and H_2O, since in both cases the $3d^n4s^1$ atomic state lies lower than the $3d^{n+1}$ state. Although the $^4F(3d^7)$ excited state of Fe^+ lies only 5·8 kcal mol^{-1} higher in energy, the bonding in the $^6A_1$ ground state of FeH_2O^+ is derived almost exclusively from the Fe^+ ground state with little contribution from the $3d^7$ occupancy. The repulsion in the $^6A_1$ high-spin ground state is reduced by 4s polarization due to sp hybridization. The most stable quartet state of FeH_2O^+ is higher in energy as the reduction in repulsion is not sufficient to pay the promotion cost. When a second water ligand bonds to the $^6A_1$ ground state of FeH_2O^+, the molecule bends to reduce the repulsion. Nevertheless, the second-ligand binding energy is only 23·5 kcal mol^{-1}.

However, the much smaller $3d^n4s^1$–$3d^{n+1}$ separation in Fe^+ than in Mn^+ results in a $^4B_{1g}$ ground state that has nearly equal contributions from the $3d^64s^1$ and $3d^7$ atomic states (Mulliken 3d population of 6·50 electrons). Thus in $Fe(H_2O)_2^+$, unlike $Mn(H_2O)_2^+$, the reduction in repulsion by promoting to the $3d^{n+1}$ state is sufficiently large to compensate for the promotion energy. Also, since the cost of promotion is amortized over two ligands, the second-ligand binding energy is actually larger than the first, in agreement with experimental observations.

The second-ligand binding energy is also larger than the first for the Cr^+, Co^+ and Cu^+ metal ions. However, since only the lowest atomic states are involved in the bonding, the 3d population is only slightly reduced when the second ligand bonds. The larger binding energy for the second ligand arises from the reduction in repulsion due to sd hybridization as illustrated in figure 1. This effect is large enough to compensate for the smaller nuclear charge felt by the second H_2O ligand due to the charge donation of the first ligand. This is analogous to what was observed for the noble-gas atoms interacting with the metal ions, except that the stronger bonding accentuates the difference in the first- and second-ligand binding energy.

The interaction of H_2O with V^+ illustrates that the orientation of the 3d electrons is an important consideration in determining the ground state. The bonding between V^+ and H_2O is much more complex than between V^+ and Ar, where the only major concern is minimizing the repulsion between the metal $3d\sigma$ orbital and Ar. The lone-pair electrons on H_2O overlap significantly with both the $3d\sigma$ and the $3d\pi$ orbitals of V^+. However, the preferred orientation of the 3d electrons is not completely determined by the repulsion. As the 3d orbitals have 'linear' symmetry, one must also consider the decomposition of a given $3d^34s^1$ occupation into the component pure atomic states. For VH_2O^+ the V^+ $3d\delta^23d\pi^14s^1$ occupancy would minimize the V^+–H_2O repulsion, but it is derived from 40% ^5F and 60% ^5P (the ^5P state is 31 kcal mol^{-1} above the ^5F). The $^5A_1$ ground state of VH_2O^+ is derived from the $3d\delta^13d\pi^24s^1$ occupancy which is 100% ^5F. Since the V^+ $3d^4$ occupancy mixes into both molecular states to about the same extent, it does not significantly affect the ordering of the two states. When the second water ligand bonds, the lower repulsion of the $3d\delta^23d\pi^14s^1$ occupancy is favoured as the promotion energy is amortized over two ligands.

The interaction of transition metals with water molecules illustrates that the ordering of the low-lying electronic states is determined by several competing mechanisms for reducing the repulsion. These include 4s-to-3d pronotion, sp and sd hybridization, and bending of the ligands. One must also consider the decomposition of the different occupancies into their component pure atomic states. The relative importance of these effects often varies between the one- and two-water-ligand cases. In many cases the repulsion can be reduced to an extent that it compensates for the smaller metal charge that the second water ligand sees, resulting in a larger binding energy for the second ligand. Since the calculated binding energies are in fairly good agreement with experiment (see table 5), we are confident that we have accounted for the most important bonding effects that make the transition-metal ions so different from the alkali ions.

3.4. *Transition-metal–CO systems*

The bonding of CO to neutral metals has been extensively discussed (Bauschlicher *et al.* 1986, Blomberg *et al.* 1988). It involves both a repulsive interaction of the CO σ orbital with the metal, and an attractive interaction due to metal $d\pi$-to-CO $2\pi^*$ donation. There is also some CO donation to the metal in the σ space. For the interaction of CO with a positive ion, the repulsive σ interaction is still very important, but the metal-to-$2\pi^*$ donation is much less important than for the neutral ion (Bauschlicher and Barnes 1988). All the factors such as hybridization, polarization and promotion that determined the binding energies of the transition-metal–water systems also affect the binding energies and nature of the bonding in the transition-metal–CO systems. We illustrate this by considering the $NiCO^+$ molecule in some detail.

Consistent with the noble-gas and water ligand studies, the lowest state of $NiCO^+$ is the $^2\Sigma^+$ state with the hole localized in the $3d\sigma$ orbital. At the SCF level the $NiOC^+$ structure is found to be 3 kcal mol^{-1} more stable than the $NiCO^+$ structure, because at this level the CO dipole moment has the wrong sign. This indicates that the electrostatic charge–dipole interaction is more important than any π bonding, which favours $NiCO^+$. At the MCPF level, the dipole moment of CO is in good agreement with experiment, which results in an $NiCO^+$ structure that is more stable than $NiOC^+$ by 11 kcal mol^{-1}. This difference is more than would be expected based solely on electrostatic arguments, indicating that electron correlation increases the importance of metal-to-ligand π donation and metal hybridization as well as improving the CO dipole moment.

The nature of the bonding and the differences with the neutral system are perhaps best illustrated by figures 3–6, where σ and π density difference plots are presented for NiCO ($^1\Sigma^+$) and $NiCO^+$ ($^2\Sigma^+$). The σ density difference plot for NiCO is shown in

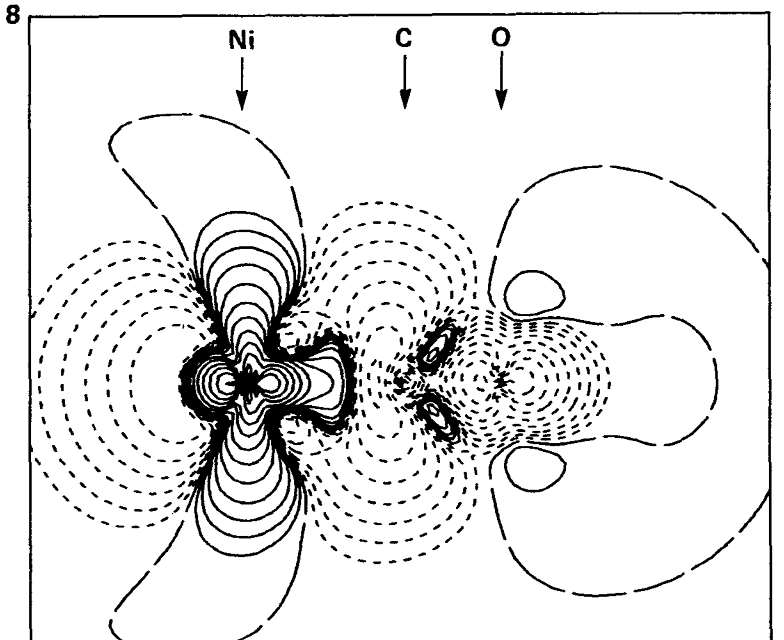

Figure 3. The σ density difference plot for NiCO $^1\Sigma^+$ minus Ni ^{1}D and CO: (——), positive contours; (- - - - -), negative contours; (— — —), zero contour.

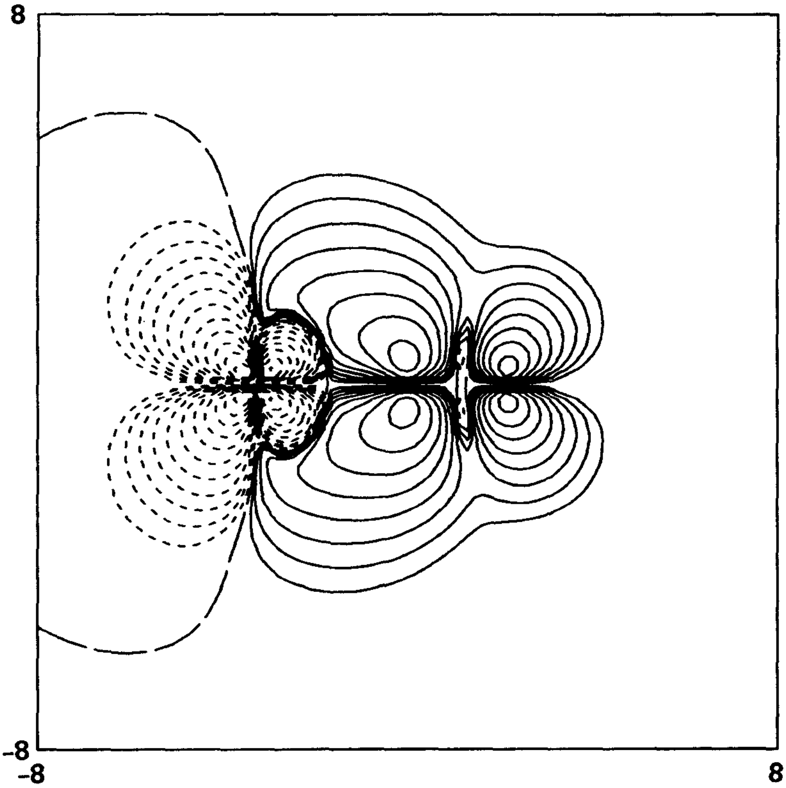

Figure 4. The π density difference plot for NiCO $^1\Sigma^+$ minus Ni ^1D and CO.

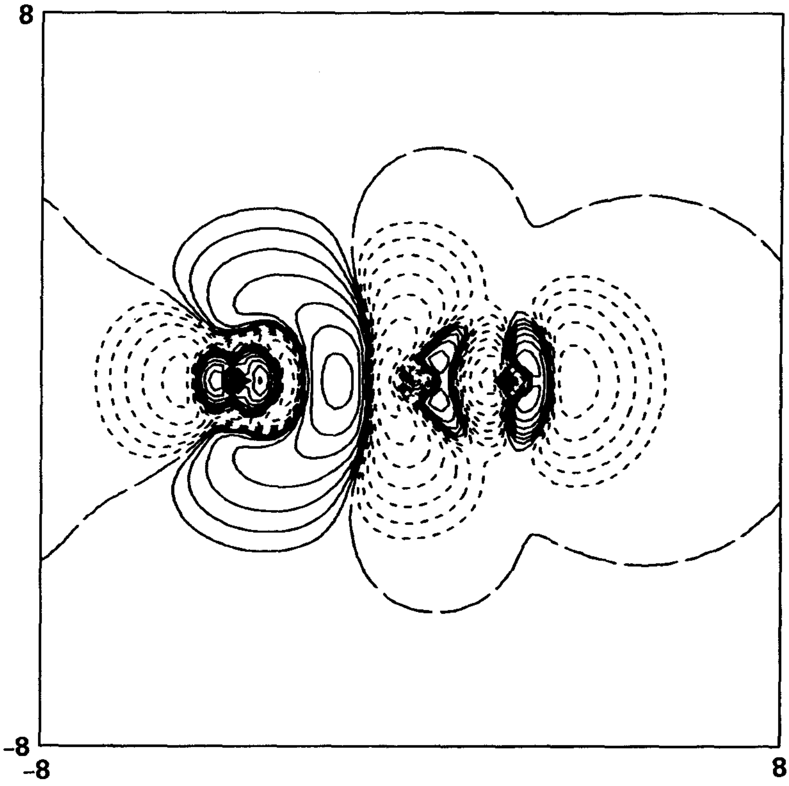

Figure 5. The σ density difference plot for NiCO$^+$ $^2\Sigma^+$ minus Ni$^+$ 3d^9 and CO.

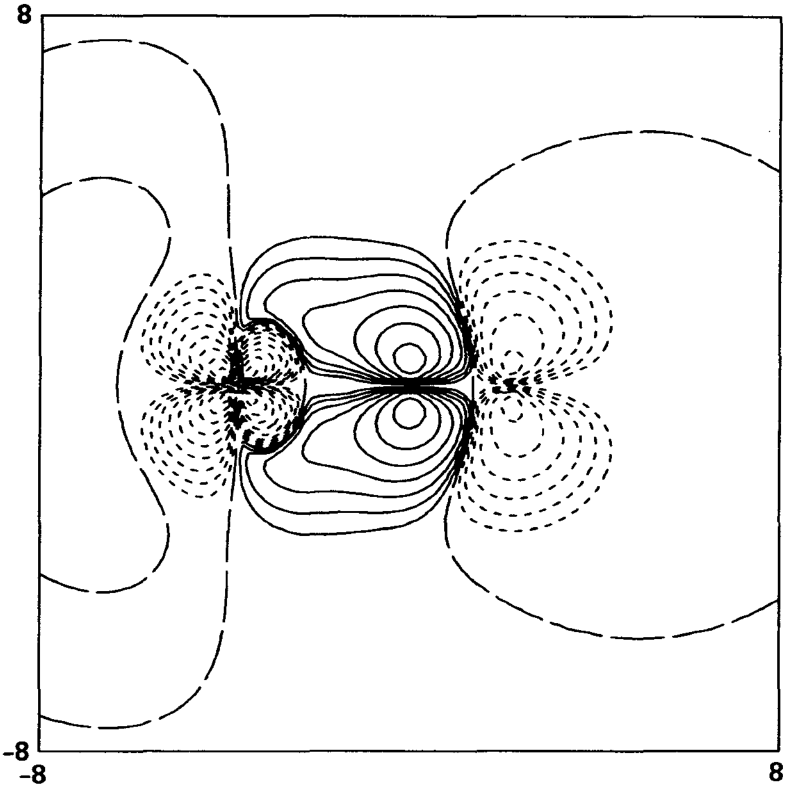

Figure 6. The π density difference plot for $NiCO^+$ $^2\Sigma^+$ minus Ni^+ $3d^9$ and CO.

figure 3. This illustrates the movement of charge density from both sides of Ni and from CO to a region centred on Ni. This is a consequence of sd hybridization, which moves charge into the 4s–3d combination of the hybrid orbital to reduce the repulsion from the region of the CO 5σ orbital. The metal-to-CO donation in the π space is clearly visible in figure 4, where we plot the π density difference for NiCO. Figures 5 and 6 give the corresponding σ and π density differences for the $^2\Sigma^+$ state of $NiCO^+$. In the σ space, the CO is polarized towards the positive charge as expected. The Ni^+ still undergoes sd hybridization as indicated by the loss of charge on the opposite side of Ni^+. However, the gain on the CO side from the CO polarization and donation is larger than the reduction by sd hybridization, giving a net increase in charge on the CO side of the Ni^+. The polarization of the CO is probably larger than for the neutral, because of the positive metal centre. The π density difference plot for $NiCO^+$ in figure 6 is very different from that for NiCO in figure 4. Since both the metal and CO polarize, there is a build-up of charge between the Ni and CO. A Mulliken population analysis shows that there are only 0·06 electrons donated to the CO 2π* orbital, which is an order of magnitude less than the 0·57 electrons donated by the neutral system.

The calculated binding energy of $NiCO^+$ at the MCPF level of 32·9 kcal mol^{-1} is significantly smaller than the experimental value (Distefano 1970) of 48 ± 2 kcal mol^{-1}. The binding energy increases by only 2 kcal mol^{-1} when the one-particle basis set is substantially expanded, indicating that the difference cannot be attributed to basis set incompleteness. Although there is some metal-to-ligand donation that is not present in the noble-gas or water ligand systems, this difference with experiment is too large to ascribe to limitations of the calculations. The experimental binding energies are determined by ionizing $Ni(CO)_n$. The ionization threshold is determined by extrapolating the measured ion intensity against photon energy to zero ion intensity. Using the ionization threshold for Ni^+, the heat of formation deduced for $Ni(CO)_4$ agrees with the thermochemical value (Fischer *et al.* 1957) to within 2 kcal mol^{-1}. However, for $NiCO^+$, the analysis is complicated by a nonlinear behaviour of the ion intensity; see figure 4 of Distefano (1970). If the long tail is assumed to be due to thermal effects, and the linear region is used to extrapolate to zero ion intensity (i.e. a photon energy of 1030 Å), the dissociation energy is computed to be $38{\cdot}8 \pm 2$ kcal mol^{-1}. This value is much more consistent with the size of the errors observed for the noble-gas or water ligand systems.

In table 6 we summarize the binding energies, the d populations and the net charges on the metal for the monocarbonyls and dicarbonyls (Barnes *et al.* 1990). With the exception of $ScCO^+$, $Mn(CO)_n^+$ and $Y(CO)_n^+$, the bonding arises from the d^{n+1} asymptote. For Mn^+ and Y^+, the d^{n+1} atomic state is apparently too high in energy to contribute to the bonding in the ground states of either the monocarbonyls or dicarbonyls. However the d^{n+1} state contributes to the bonding in $Sc(CO)_2^+$, because promotion becomes favourable when amortized over two ligands. The $Sc(CO)_2^+$ molecule has a $\pi^2(^3\Sigma^-)$ ground state even though this is derived from 80% ^3F and 20% excited ^3P, since this maximizes dπ-to-CO $2\pi^*$ donation. The $Y(CO)_2^+$ molecule is linear despite the very large 5s population, apparently because sd hybridization is very favourable as a result of the comparable radial extent of the 4d and 5s orbitals. In fact, the only dicarbonyl ion that is bent is $Mn(CO)_2^+$. Since the bonding arises exclusively from the $3d^54s^1$ atomic state, the molecule cannot sd hybridize to reduce repulsion. Thus the molecule becomes strongly bent so that some sp hybridization can occur to reduce the repulsion. Although bending increases the second binding energy by 5·2 kcal mol^{-1}, the second-ligand binding energy is still less than the first, and $Mn(CO)_2^+$ has the smallest binding energy of any dicarbonyl in either the first or second transition row.

It is interesting to contrast the bonding in $FeCO^+$, FeH_2O^+ and $FeAr^+$. The $FeCO^+$ molecule has a $^4\Sigma^-$ ground state with a $3d\sigma^1 3d\pi^4 3d\delta^2$ occupation, whereas both FeH_2O^+ and $FeAr^+$ have a sextet ground state derived from the $3d^64s^1$ occupation. The electrostatic interaction is smaller in $FeCO^+$ than in FeH_2O^+, because of the smaller dipole moment of CO. For the molecule to achieve a favourable overlap of the CO $2\pi^*$ orbital with the $3d\pi$ orbital of Fe^+ a short bond distance is required. This increases the desirability of promoting the 4s electron into the 3d shell to reduce the repulsion. For FeH_2O^+ and $FeAr^+$, the metal d electrons are oriented to minimize repulsion, whereas for $FeCO^+$ the d electrons orient both to minimize the σ repulsion and to maximize π donation.

The binding energies for the monocarbonyl and dicarbonyl ions are largest when the metal ion has a d^{n+1} ground state. Otherwise the molecule has either to pay the promotion energy or to incur the repulsive interaction of the metal valence s electron. The binding energies for the half-filled d shells (Cr^+ and Mo^+) and filled d shells (Cu^+ and Ag^+) are somewhat less, because an electron is being added in each case to the $3d\sigma$ orbital. The binding energy of $AgCO^+$ is notably smaller than $CuCO^+$ because the much larger $4d^{10}$–$4d^95s^1$ separation in Ag^+ precludes any sd_σ hybridization to reduce the repulsion with the CO 5σ orbital and the stability of the $4d^{10}$ closed-shell occupancy minimizes any donation to the $2\pi^*$ orbital.

Table 6. Binding energies and metal d and net populations for the ground states of the $M(CO)_n^+$ molecules.

	$M(CO)_2^+$				$M(CO)^+$				
	State	D_e (kcal mol^{-1})	d population	Net population	State	D_e (kcal mol^{-1})	d population	Net population	Δ† (kcal mol^{-1})
Sc	$^3\Sigma_g^-$	25·0	1·75	0·89	$^3\Delta$	12·7	1·16	0·85	−0·4
Ti	$^4\Delta_g$	38·9	2·91	0·79	$^4\Delta$	20·2	2·89	0·92	−1·5
V	$^5\Delta_g$	44·7	3·67	0·66	$^5\Sigma^+$	23·6	3·98	0·87	−2·5
Cr	$^6\Sigma_g^+$	38·6	4·82	0·64	$^6\Sigma^+$	18·8	4·90	0·84	+1·0
Mn	$^7A_1$‡	17·5	5·03	0·75	$^7\Sigma^+$	10·2	5·01	0·87	−2·9
Fe	$^4\Sigma_g^-$	53·0	6·77	0·52	$^4\Sigma^-$	21·9	6·77	0·83	+9·2
Co	$^3\Delta_g$	64·2	7·85	0·49	$^3\Delta$	33·1	7·86	0·79	−2·0
Ni	$^2\Sigma_g^+$	63·9	8·91	0·45	$^2\Sigma^+$	32·9	8·93	0·76	−1·9
Cu	$^1\Sigma_g^+$	59·8	9·79	0·34	$^1\Sigma^+$	29·0	9·87	0·75	+1·8
Y	$^1\Sigma_g^+$	24·0	0·79	0·75	$^1\Sigma^+$	11·6	0·56	0·84	+0·8
Zr	$^4\Delta_g$	43·7	2·84	0·92	$^4\Delta$	24·2	2·87	0·96	−4·7
Nb	$^5\Sigma_g^+$	49·3	3·96	0·81	$^5\Sigma^+$	28·6	3·97	0·89	−7·9
Mo	$^6\Sigma_g^+$	39·9	4·72	0·68	$^6\Sigma^+$	18·8	4·83	0·83	+2·3
Tc	$^5\Pi_g$	35·7	5·67	0·68	$^5\Pi$	8·8	5·73	0·84	+18·1
Ru	$^4\Sigma_g^-$	59·9	6·70	0·63	$^4\Sigma^-$	30·9	6·76	0·80	−1·9
Rh	$^3\Delta_g$	58·9	7·85	0·55	$^3\Delta$	30·8	7·88	0·77	−2·7
Pd	$^2\Sigma_g^+$	59·1	8·93	0·52	$^2\Sigma^+$	31·5	8·94	0·76	−3·9
Ag	$^1\Sigma_g^+$	38·7	9·79	0·65	$^1\Sigma^+$	19·2	9·96	0·90	+0·3

† Computed as $D_e[M(CO)_2^+]-2D_e[MCO^+]$.

‡ The calculated bond angle is 82·4°.

In contrast with the transition-metal–noble-gas and transition-metal–water systems, the second CO is bound by slightly less than the first for many of the transition metals. The Mulliken population analysis suggests that the positive charge on the metal ion minimizes the donation of charge density from the metal dπ orbital into the CO $2\pi^*$ orbital. This effect is accentuated when two CO ligands are present, resulting in an even smaller donation per CO. The Fe^+ and Tc^+ metal ions are two exceptions where the second-ligand binding energy is significantly larger than the first. This arises because the cost of promotion can be amortized over both ligands. For Sc^+ and Y^+ there is an increase in the d population with the second CO ligand, but the sharing of the promotion energy leads to only a small enhancement of the second-ligand binding energy for Y^+ and a small decrease for Sc^+.

The theoretical results for the monocarbonyls and dicarbonyls provide a systematic and, we believe, accurate set of data for comparison with experiment. The calculated $Co–CO^+$ binding energy of 33·1 kcal mol^{-1} is in good agreement with the experimental value of 30·1 kcal mol^{-1} (Hanratty *et al.* 1988). This provides further support for the contention that the experimental value for $NiCO^+$ is too large. For $FeCO^+$, our calculated value of 21·9 kcal mol^{-1} is estimated to be 3·5 kcal mol^{-1} too small because of errors in the Fe^+ ion separations and up to 4 kcal mol^{-1} too small owing to limitations in the basis set and correlation treatment. Thus our best estimate of about 30 kcal mol^{-1} for $Fe–CO^+$ is less than most of the experimental determinations, which range from 38 to 61 kcal mol^{-1} (Halle *et al.* 1984, Distefano 1970, Cassady and Freiser 1984). Clearly a systematic experimental study of the monocarbonyls and dicarbonyls for a variety of transition metals would be very worthwhile as a critical test of the theoretical binding energies and explanations of the observed trends.

3.5. *Transition-metal hydride systems*

The transition-metal–H and transition-metal–CH_3 bonds are so similar in character that we consider these systems together (Chong *et al.* 1986, Langhoff *et al.* 1987, Pettersson *et al.* 1987, Bauschlicher *et al.* 1989b, Rosi *et al.* 1990). However, many aspects of the bonding in MH^+ and $M(CH_3)_n^+$ are different from the mechanisms discussed above, because the bonding is covalent, as for the neutral systems. The bonds vary considerably in the degree of d character, since this depends on the degree of sd hybridization and s-to-d promotion, which in turn depends on the d^ns^1–d^{n+1} atomic separation. Also note that, for the neutral systems and for Y^+, the s^2 atomic asymptote can contribute to the bonding through either sd or sp hybridization. This mixing of asymptotes is one of the important components in a set of 'rules' that were developed (Walch and Bauschlicher 1983) to predict the ground states of these molecular systems. Therefore, differences in the bonding for the first- and second-transition-row metal atoms can generally be related to changes in the ordering of the atomic states.

In table 7 we summarize the structures and selected populations for the ground states of the MH^+ and MCH_3^+ ions. The d populations reflect the fact that the bonding generally arises from a mixture of atomic states. We note that, while the MCH_3^+ molecules have C_{3v} symmetry, in most cases the d orbitals can be classified according to linear symmetry and can therefore be directly compared with the MH^+ states. This preservation of high local symmetry is sufficient to allow separate SCF optimizations for $^2\Delta$ and $^2\Pi$-like ^2E states of $ScCH_3^+$. The MCH_3^+ and MH^+ ions have the same ground state for all the metals except Ti and Nb. In $TiCH_3^+$ and $NbCH_3^+$ we find that the dδ and dπ orbitals mix strongly and destroy the local high symmetry. This allows

Table 7. Spectroscopic constants and metal d and net populations for the MH^+ and MCH_3^+ molecules.

	MH^+				MCH_3^+†				
	State	r_e (units of a_0)	d population	Net population	State	r(M–C) (units of a_0)	<MCH (degrees)	d population	Net population
Sc	$^2\Delta$	3·457	1·29	1·23	^2E	4·158	111·4	1·34	1·25
Ti	$^3\Phi$	3·289	2·34	1·11	$^3A_2$	4·017	110·9	2·37	1·21
V	$^4\Delta$	3·143	3·37	1·01	^4E	3·960	110·6	3·37	1·19
Cr	$^5\Sigma^+$	3·031	4·45	0·91	$^5A_1$	3·815	109·2	4·53	1·12
Mn	$^6\Sigma^+$	3·122	5·10	0·85	$^6A_1$	3·942	107·4	5·11	1·06
Fe	$^5\Delta$	3·029	6·19	0·78	^5E	3·808	107·4	6·21	1·02
Co	$^4\Phi$	2·923	7·22	0·74	^4E	3·655	107·5	7·21	0·98
Ni	$^3\Delta$	2·810	8·26	0·73	^3E	3·675	106·6	8·24	0·95
Cu	$^2\Sigma^+$	2·730	9·45	0·48	$^2A_1$	3·932	99·1	9·86	0·82
Y	$^2\Sigma^+$	3·576	0·80	1·00	$^2A_1$	4·265	111·0	0·81	1·12
Zr	$^3\Delta$	3·459	1·97	1·10	^3E	4·097	109·5	2·00	1·09
Nb	$^4\Delta$	3·295	3·57	1·09	$^4A_2$	3·995	108·2	3·13	1·04
Mo	$^5\Sigma^+$	3·174	4·72	0·95	$^5A_1$	3·979	108·5	4·71	1·09
Tc	$^6\Sigma^+$	3·198	5·18	1·00	$^6A_1$	3·969	107·5	5·18	1·06
Ru	$^5\Delta$	3·158	6·35	0·95	^5E	3·946	105·8	6·39	0·97
Rh	$^2\Delta$	2·864	7·99	0·77	^2E	3·873	104·7	7·99	0·87
Pd	$^1\Sigma^+$	2·817	9·03	0·69	$^1A_1$	3·793	103·4	9·05	0·81
Ag	$^2\Sigma^+$	3·442	9·83	0·88	$^2A_1$	4·539	97·3	9·87	0·86

† The C–H bond distance is fixed at $2{\cdot}07a_0$.

several 'linear' states to mix together, giving a mixed state of lower energy than expected by analogy with MH^+. This stabilization is a relatively small effect; so the 'expected' ground state in analogy with MH^+ is only slightly higher in energy.

While the bondings in MH^+ and MCH_3^+ are very similar, the first and second transition rows are very different. The hydride ground states are different for Y and Sc, Zr and Ti, Rh and Co, and Pd and Ni. NiH^+ and CoH^+ are both derived from the d^ns^1 asymptote, while the greater stability of the 4d orbitals relative to the 3d orbitals results in Rh and Pd being derived from the d^{n+1} asymptote. The difference between ScH^+ and YH^+ is easily explained by the change from a $^3D(3d^14s^1)$ ground state in Sc^+ to a $^1S(5s^2)$ ground state in Y^+. The change in ground state between TiH^+ and ZrH^+ illustrates the fact that the radial extent of the 4d and 5s orbitals is more similar than the 3d and 4s orbitals. Thus sd hybridization is more favourable for Zr than for Ti and, when coupled with the slightly larger d^ns^1–d^{n+1} splitting in Zr^+, this results in a change in the ground state. The difference between the bonding in the first and second transition row is also apparent in the composition of the bonding orbital (table 8) where a large increase in the d contribution in the bonding is visible, especially for the second half of the row.

The Mulliken d populations should be reliable, since the compact nature of the d orbitals results in very small overlap populations. Although the valence populations are subject to larger population artefacts, the computed trends are expected to be

Table 8. Decomposition of the MCPF bonding orbital based on Mulliken populations of the natural orbitals for the monomethyl neutrals and ions.

	Population (%) for ions			Population (%) for neutrals		
	4s+4p	3d	Metal	4s+4p	3d	Metal
Sc	16	21	37	12	16	29
Ti	18	15	33	15	9	24
V	22	17	39	16	10	26
Cr	15	24	40	15	13	29
Mn	31	13	44	23	6	29
Fe	25	22	47	31	5	35
Co	26	24	51	39	2	41
Ni	24	29	53	46	0	46
Cu†	24	7	31	37	1	38
	Population (%) for ions			Population (%) for neutrals		
	5s+5p	4d	Metal	5s+5p	4d	Metal
Y	13	21	35	10	17	27
Zr	11	27	38	9	22	32
Nb	11	30	41	13	19	32
Mo	8	35	43	14	20	34
Tc	13	36	49	31	11	42
Ru	6	54	59	9	32	42
Rh	3	55	58	11	33	44
Pd	2	59	62	5	46	52
Ag†	19	2	21	39	0	40

† For the ion, this is the composition of the singly occupied orbital.

Table 9. D_0 values for the MH^+ and MCH_3^+ molecules. Experimental values are taken from the recent review of the literature by Armentrout and Georgiadis (1988); the values (with uncertainties in parentheses) have been converted from 300 to 0 K.

	D_0 (kcal mol^{-1})			
	Ab initio		Experiment	
	CH_3	H	CH_3	H
Sc	52·4	56·0	57·5 (3·0)	55·4 (2·1)†
Ti	51·6	53·3	56·0 (2·8)	53·3 (2·5)
V	43·0	48·6	48·5 (2·3)	47·3 (1·4)
Cr	25·5	27·7	28·7 (2·3)	31·6 (2·0)
Mn	43·7	43·7	50 (5)	47·5 (3·4)
Fe	53·1	52·3	56·4 (2·4)	48·9 (1·4)
Co	48·3	44·5	48 (4)†	45·7 (1·4)
Ni	39·8	41·0	44 (3)†	38·6 (1·8)
Cu	28·8	18·5	28·2 (1·7)†	21·2 (3·0)
Y	58·6	59·4	58·0 (1·2)†	60·2 (1·4)†
Zr	57·3	56·7		54 (3)
Nb	49·5	52·5		53 (3)
Mo	31·9	35·3		41 (3)
Tc	47·7	50·7		
Ru	39·6	37·8	53 (5)	40 (3)
Rh	37·1	41·5	46 (5)	35 (3)
Pd	47·2	49·0	58 (5)	46 (3)
Ag	21·9	10·6		15 (3)

† Revised values (P. B. Armentrout 1989, private communication).

reliable, because of the similar one-particle basis sets employed for each of the transition metals. The net charge on the metal is larger than one for the early metals but decreases with increasing Z. Hence, there is metal-to-H and metal-to-CH_3 donation on the left-hand side of the row, but this changes to H-to-metal and CH_3-to-metal donation towards the end of the row. This charge donation also affects the variation in the M–C–H angle in MCH_3^+. The energy of the planar CH_3 structures relative to the one where the hydrogen atoms are bent 22° out of the plane shows that bending destabilizes CH_3^+ and CH_3 by 40 and 8 kcal mol^{-1} respectively, but CH_3^- is stabilized by 8 kcal mol^{-1}. The change in bond angle is largest for Ag and Cu, where the metals are d^{10} and hence the bonding mechanism is mostly CH_3-to-metal donation.

In table 9 we compare our best D_0 values for MH^+ and MCH_3^+ with experiment. These values include a correction (up to about 6 kcal mol^{-1}), which accounts for the estimated errors remaining in the calculations. Overall the computed values agree well with experiment. There is a significant difference only for $RuCH_3^+$, $RhCH_3^+$ and $PdCH_3^+$. Given that the calculations are expected to be of about the same accuracy for all the systems, and given the similarity of the methyls and hydrides, we conclude that the experimental D_0 values (Mandich *et al.* 1984) for $RuCH_3^+$, $RhCH_3^+$ and $PdCH_3^+$ are systematically too large.

Although there are many similarities between the neutrals and positive ions, there are some notable differences as well. In table 8 we compare the decomposition of the bonding orbital for the neutral and positive transition-metal methyls. The bonding orbital has more metal character for the ion since it is less willing to give up electrons. There is also less d character in the bond for the neutral as the additional electron resides primarily in the s orbital.

On the basis of selected experimental D_0 values, it has been proposed (Mandich *et al.* 1984) that the binding energies of the neutral hydrides are about 10 kcal mol^{-1} stronger than the methyls, but that the greater polarization in the methyl group results in approximately equal binding energies for the hydride and methyl ions. In table 10 we compare the D_0 values for the hydrides and methyls as well as comparing the ions with the neutrals. The theoretical results indicate that, while the above arguments are approximately true for the late elements, it is not true for those at the beginning of each row.

The good agreement between the calculated and experimental binding energies for the hydride and methyl positive ions supports the validity of the theoretical methods employed. Since the theoretical results provide a consistent set of values, they can potentially identify incorrect experimental values. Also, unlike experiment, the calculations should have approximately equal accuracy for the neutrals and ions. Thus the theoretical results for the neutrals should be the most accurate (and consistent) set at present available.

In table 11 we summarize the results of calculations for the dimethyl positive ions $M(CH_3)_2^+$. We have optimized the geometry assuming two M–CH_3 bonds. At the MCPF level of theory the C–C bond energy in C_2H_6 is about 90 kcal mol^{-1}. Thus metal ions which have $M(CH_3)_2^+$ binding energies of less than about 90 kcal mol^{-1} do not insert into the C–C bond. Instead, the equilibrium structures involve a complex where the M^+ is electrostatically bonded to a slightly perturbed C_2H_6 molecule. For

Table 10. Comparison of the neutral and ion D_0 values for the MH and MCH_3 molecules. The second difference is defined as $[(D_0(MCH_3^+)-D_0(MH^+)]-[D_0(MCH_3)-D_0(MH)]$.

	Positive ions			Neutrals			
	D_0 (kcal mol^{-1})		Δ (kcal mol^{-1})	D_0 (kcal mol^{-1})		Δ (kcal mol^{-1})	Second difference (kcal mol^{-1})
	CH_3	H		CH_3	H		
Sc	52·4	56·0	3·6	48·7	51·1	2·4	−1·2
Ti	51·6	53·3	1·7	40·4	46·3	5·9	4·2
V	43·0	48·6	5·6	44·5	52·4	7·9	2·3
Cr	25·5	27·7	2·2	37·7	47·8	10·1	7·9
Mn	43·7	43·7	0·0	28·4	38·3	9·9	9·9
Fe	53·1	52·3	−0·8	33·7	37·8	4·1	4·9
Co	48·3	44·5	−3·8	38·4	44·1	5·7	9·5
Ni	39·8	41·0	1·2	52·2	61·2	8·8	7·6
Cu	28·8	18·5	−10·0	49·0	60·0	11·0	21·0
Y	58·6	59·4	0·8	61·8	66·8	5·0	4·2
Zr	57·3	56·7	−0·6	53·3	55·4	2·1	2·7
Nb	49·5	52·5	3·0	50·8	58·7	8·9	5·9
Mo	31·9	35·3	3·4	40·3	49·2	8·9	5·5
Tc	47·7	50·7	3·0	38·3	44·4	6·1	3·1
Ru	39·6	37·8	−1·8	40·5	53·4	12·9	14·7
Rh	37·1	41·5	4·4	49·3	63·9	14·6	10·2
Pd	47·2	49·0	1·8	37·6	50·4	12·8	11·1
Ag	21·9	10·6	−11·3	37·8	50·8	13·0	24·3

Table 11. Equilibrium geometries, populations and dissociation energies for the ground states of the $M(CH_3)_2^+$ ions. Δ is computed as $D_e\,[M(CH_3)_2^+] - 2D_e[MCH_3^+]$.

	State	r(M–C) (units of a_0)	<CMC (degrees)	d population	Net population	D_e (kcal mol^{-1})	Δ (kcal mol^{-1})
Sc	$^1A_1$	4·027	106·5	1·05	1·33	108·0	+5·0
Ti	$^2A_1$	3·898	105·8	2·15	1·18	95·8	−5·8
V	$^3A_2$	3·808	108·6	3·30	1·14	86·9	+0·3
Cr	$^4B_2$	3·767	110·6	4·42	1·10	46·6	+1·8
Mn	$^5B_2$	3·827	96·3	5·24	1·01	67·3	−14·5
Fe	$^4B_2$	3·732	97·0	6·28	0·94	83·9	−17·9
Co	$^3B_1$	3·753	101·2	7·38	0·86	87·7	−9·5
Ni	$^2A_1$	3·571	91·2	8·48	0·80	85·0	+6·6
Cu	$^1A_1$	3·749	90·9	9·48	0·70	65·9	+15·1
Y	$^1A_1$	4·343	105·7	1·01	1·37	116·8	−2·4
Zr	$^2A_1$	4·120	101·8	2·00	1·22	122·1	+6·3
Nb	$^3A_2$	4·035	97·0	3·22	1·13	101·1	+5·9
Mo	$^4B_2$	3·952	115·2	4·50	1·15	67·5	+7·3
Tc	$^5B_2$	3·928	96·8	5·25	1·08	90·1	−1·3
Ru	$^4B_2$	3·861	106·8	6·43	0·95	85·8	+5·6
Rh	$^3B_1$	3·875	105·4	7·54	0·87	80·6	+7·2
Pd	$^2A_1$	3·835	93·5	8·73	0·77	82·9	−10·7
Ag	$^1A_1$	4·056	80·6	9·60	0·80	46·8	+9·4

example, the Ag^+ ion interacts with two of the hydrogen atoms and is bound by about 12 kcal mol^{-1}. However, even though the structure with two M–C bonds is unstable for some ions, we have still carried out a systematic study of all the systems to contrast the bonding for the different transition-metal ions.

All the systems with two M–C bonds are bent, since the bonding involves covalent bonds of the methyls with sd hybrid orbitals on the metal leading to an angle of approximately 90°. It is interesting to note that, for some dihydrides such as MoH_2^+, a small-angle structure, where the H_2 retains some H–H bonding, is very stable because it interacts with two different d orbitals (Schilling *et al.* 1987b). However, the greater directionality of the M–C bond precludes similar structures for the dimethyl positive ions. Unlike the monomethyls, we find the same ground states for the corresponding first- and second-row ions. We believe that this is a consequence of the fact that the bonding arises mostly from the d^ns^1 occupancy in all the systems. Excluding Cu^+ and Ag^+, the M–C bond lengths are similar for the monomethyl and dimethyl ions. Since Cu^+ and Ag^+ have d^{10} ground states, the bonding in the monomethyl systems primarily involves a one-electron bond with the electron coming from the methyl group. Two-electron bonds are energetically unfavourable, because of the high cost of promoting to the d^9s^1 occupancy. However, for the dimethyl case, the promotion cost is shared, so that two two-electron bonds form, resulting in much stronger bonding.

Several other transition-metal dimethyls have a large difference between the first and second binding energy that can be understood in terms of the promotion energy required to form the second bond. For example, Pd^+ has a $4d^9$ occupancy while Mn^+ and Fe^+ have $3d^n4s^1$ occupancies. Therefore, each ion can form one strong bond without rehybridizing but must pay some promotion energy to form the second bond, which generally makes the second binding energy much less than the first. The bond energy for the second methyl is less than the first in $Co(CH_3)_2^+$, because of the loss of exchange energy with the second bond. The M–C–H angles in $M(CH_3)_2^+$ show the same decrease with increasing Z as for the MCH_3^+ ions. Again this occurs because on the left-hand side of the row there is metal-to-CH_3 donation which decreases in magnitude, eventually becoming CH_3-to-metal donation by the end of the row.

3.6. *La^+ and La^{2+} interacting with hydrocarbons*

In this section we study the interaction of La^+ and La^{2+} with C_2H_2, C_2H_4 and C_3H_6, motivated in part by recent experiments by T. J. MacMahon and B. S. Freiser (1989, private communication). An interesting observation of the experimental studies was that the singly charged ions were more strongly bound than the doubly charged species. For example, the La^+–C_2H_2 binding energy was found to be $38 \pm 6\,\mathrm{kcal\,mol^{-1}}$ compared with a La^{2+}–C_2H_2 binding energy of $33 \pm 6\,\mathrm{kcal\,mol^{-1}}$. The difference in dissociation energy for C_3H_6 was even larger: $63 \pm 6\,\mathrm{kcal\,mol^{-1}}$ for La^+ and $41 \pm 6\,\mathrm{kcal\,mol^{-1}}$ for La^{2+}. This implies that the bonding is not simply electrostatic, since otherwise La^{2+} would bind by about twice as much as La^+. Sunderlin and Armentrout (1989) have also studied the bonding of La^+ with C_2H_2, but their lower bound of $65\,\mathrm{kcal\,mol^{-1}}$ for the binding energy is much larger than the value of MacMahon and Freiser. This implies an even larger difference between the monocation and dication binding energies. They also determined a lower bound of $23{\cdot}3\,\mathrm{kcal\,mol^{-1}}$ for the binding energy of $LaC_2H_4^+$.

A series of calculations were undertaken to understand these experimental measurements (Rosi and Bauschlicher 1990). The optimal structures and binding energies for La^+ and La^{2+} reacting with C_2H_2 and C_2H_4 are summarized in table 12. The optimal structures for $LaC_3H_6^+$ are given in figure 7. For $LaC_2H_2^+$ we find a $^1A_1$ ground state where the La^+ $5d^2$ has inserted into the in-plane π bond to form a three-membered ring. The C–C bond length in $LaC_2H_2^+$ is characteristic of a double bond, being similar to that for isolated C_2H_4. The H–C–C angle indicates sp^2 hybridization. The binding energy of the $^3B_1$ state is about half that for the $^1A_1$ state, because there is no chemical bond. Instead the bonding is mostly electrostatic in origin, although there is some donation of the La^+ 5d electrons into the π^* orbitals of C_2H_2. The ground state of $LaC_2H_2^{2+}$ is found to be of $^2B_2$ symmetry, where the sole La^{2+} 5d electron donates into the in-plane π^* orbital. However, the donation is small and the bonding is essentially electrostatic in origin. The binding energy of the $^2B_2$ state of $LaC_2H_2^{2+}$ is

Table 12. MCPF results for the geometries and the binding energies for La^+ and La^{2+} interacting with C_2H_2 and C_2H_4. BMP is the bond midpoint of the C–C bond. H-bend is the angle for H bending away from the La.

	State	r(C–C) (Å)	r(C–H) (Å)	<HCH (degrees)	r(La–BMP) (Å)	H-bend (degrees)	Binding energy (kcal mol^{-1})
C_2H_2		1·24	1·08				
C_2H_4		1·38	1·10	116·8			
C_2H_6		1·57	1·11	108·0			
$LaC_2H_2^+$	$^1A_1$	1·36	1·09		2·26	50·1	50·5
$LaC_2H_2^+$	$^3B_1$	1·29	1·08		2·52	32·5	25·1
$LaC_2H_2^{2+}$	$^2B_2$	1·27	1·08		2·63	24·4	38·4
$LaC_2H_4^+$	$^1A_1$	1·54	1·11	111·8	2·30	19·6	30·7
$LaC_2H_4^{2+}$	$^2B_2$	1·41	1·10	116·5	2·96	6·8	36·4

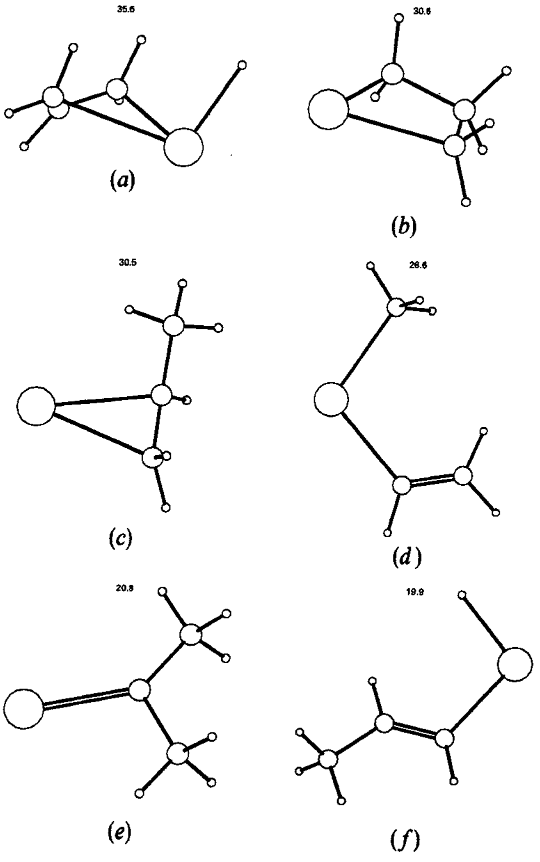

Figure 7. The stationary points for the $LaC_3H_6^+$ molecule.

larger than for the $^3B_1$ state of $LaC_2H_2^+$, since the bonding is electrostatic in both ions. Thus it is the chemical bonding in the $^1A_1$ state that leads to a larger binding energy for the singly charged ion than for the doubly charged ion. However, the calculated difference between the $LaC_2H_2^+$ and $LaC_2H_2^{2+}$ binding energies is larger than measured by MacMahon and Freiser.

The bonding in the $^1A_1$ ground state of $LaC_2H_4^+$ is similar to that in $LaC_2H_2^+$. The C–C bond distance in $LaC_2H_4^+$ indicates that only a single bond remains after La inserts into the π bond. The C–C–H angle is consistent with sp^3 hybridization. While the natures of the bonding are similar in $LaC_2H_2^+$ and $LaC_2H_4^+$, the binding energy is smaller in $LaC_2H_4^+$, since it takes 28 kcal mol^{-1} more energy to break a π bond in C_2H_4 than in C_2H_2. In contrast, $LaC_2H_2^{2+}$ and $LaC_2H_4^{2+}$ have similar binding energies, since the interaction is electrostatic and the two hydrocarbons can relax and stabilize the dication by similar amounts.

The binding energy of $LaC_3H_6^{2+}$ is predicted to be 4 kcal mol^{-1} more than $LaC_2H_2^{2+}$, which is consistent with the larger relaxation energy of the larger hydrocarbon. This increase in binding is also observed experimentally. For the interaction of La^+ with C_3H_6 we have considered several structures (see figure 7). The allyl-like structure in figure 7 (*a*) is the most stable. The four-membered ring structure in figure 7 (*b*) is 5 kcal mol^{-1} less stable, and differs from that in figure 7 (*a*) by the migration of a H from La to the central carbon. The structure in figure 7(*c*) has essentially the same binding energy as that in figure 7(*b*). This structure corresponds to La inserting into the C–C double bond. This structure has a similar bonding mechanism and binding energy to the $^1A_1$ state of $LaC_2H_4^+$. Inserting La^+ into the C–C single bond to produce the structure in figure 7(*d*) is less favourable, as is the rearrangement to form a La–C double bond (figure 7(*e*)). Inserting the La^+ into a C–H bond is very unfavourable (figure 7(*f*)), having about half of the binding energy of the most stable structure. Note that no stable geometry was found for inserting La^+ into the C–H bond of the CH_3 group: it collapsed to the structure in figure 7(*a*).

The theoretical results for the binding energies of La^+ and La^{2+} interacting with hydrocarbons allows us to comment critically on the experimental measurements. For La^+–C_2H_2 our computed binding energy is 15 kcal mol^{-1} larger than the value of MacMahon and Freiser, but 12 kcal mol^{-1} smaller than the value of Sunderlin and Armentrout. Since the theoretical value could be as much as 10 kcal mol^{-1} too small, we conclude that the value of Sunderlin and Armentrout is more accurate. Our computed La^{2+}–C_2H_2 binding energy should be more reliable (an error of about 5 kcal mol^{-1}), since the electrostatic bonding is easier to describe. Thus the theoretical binding energy suggests that the experimentally measured value of MacMahon and Freiser is slightly too small. The difference between the theoretical binding energies for La^+ interacting with C_2H_4 and C_2H_2 is consistent with the fact that it is harder to break the π bond in C_2H_4 than in C_2H_2. However, the difference between the Sunderlin and Armentrout experimental values for $LaC_2H_2^+$ and $LaC_2H_4^+$ of 39 kcal mol^{-1} is inconsistent with this observation. Thus it is likely that their lower bound for the binding energy of $LaC_2H_4^+$ is at least 10 kcal mol^{-1} too small. The theoretical value for the binding energy of $LaC_3H_6^{2+}$ is in good agreement with experiment. Since the bonding is electrostatic, the theoretical value is expected to be only slightly too small. The theoretical binding energy for $LaC_3H_6^+$ is significantly smaller than the value deduced from experiment. Since our error should not exceed 10 kcal mol^{-1}, theory supports a binding energy of less than 50 kcal mol^{-1}. Freiser and co-workers are currently performing additional experiments to resolve the differences between theory and experiment. Further, both theory and experiment are being extended to consider the Sc and Y analogues, as well as considering additional hydrocarbons.

3.7. *Diatomic metal dications*

The La^{2+}–ligand bonding described in the previous section was electrostatic in origin, but chemical bonding is also possible for dications. In most cases the molecular system is metastable, with the molecular well being above the asymptote. However, the large barriers to dissociation make these systems effectively stable. In this section we consider such bonding, for both the homonuclear Be_2^{2+} and the heteronuclear $LaFe^{2+}$, $LaRu^{2+}$ and YRu^{2+} dications.

In figure 8 we plot the potential curves for the $^1\Sigma_g^+$, $^1\Sigma_u^+$, $^1\Pi_u$ and $^3\Pi_u$ states of Be_2^{2+} from Bauschlicher and Rosi (1990). The X $^1\Sigma_g^+$ ground state, which is derived from the $^2S+{}^2S$ asymptote, forms a single two-electron bond with a bond length of $4{\cdot}025a_0$. Thus a single bond is sufficient to overcome the Coulomb repulsion. Although the minimum in the well is 2·36 eV above the $Be^+ + Be^+$ asymptote, the X $^1\Sigma_g^+$ state is long lived owing to the 1·11 eV barrier to dissociation (the maximum occurring at $6{\cdot}61a_0$). The large barrier results in a lifetime with respect to unimolecular decay of $1{\cdot}33 \times 10^{93}$ s for the lowest vibrational level in the Wentzel–Kramers–Brillouin approximation. In

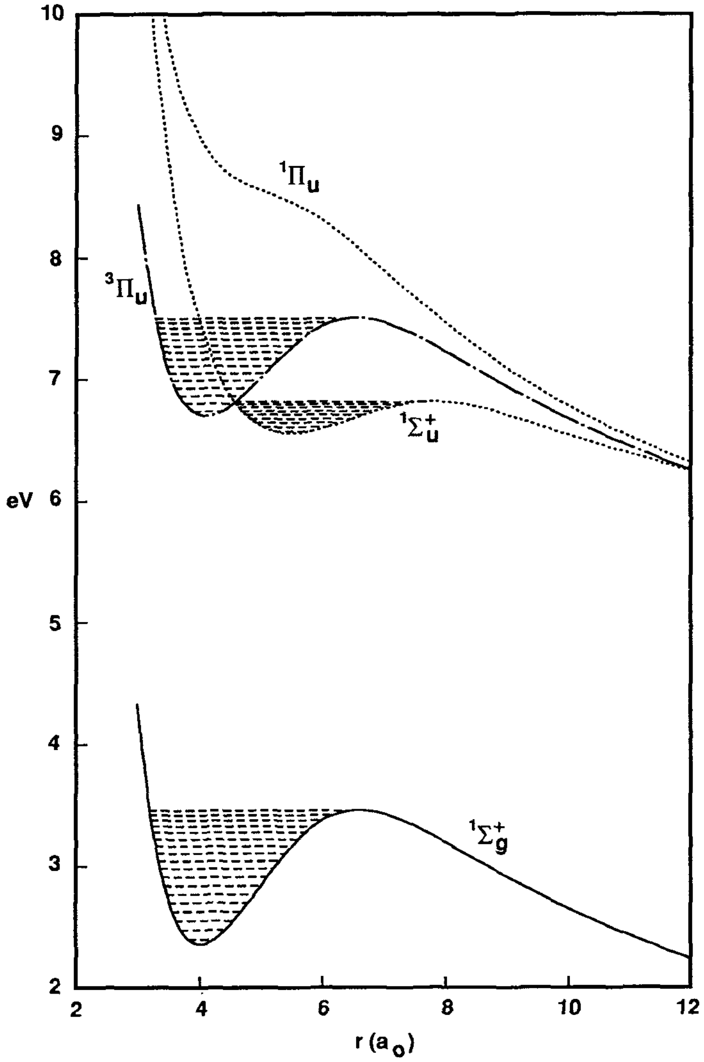

Figure 8. The $^1\Sigma_g^+$, $^1\Sigma_u^+$, $^3\Pi_u$ and $^1\Pi_u$ states of Be_2^{2+}. The zero of energy is $Be^+ + Be^+$.

fact, the theoretical potential supports 13 vibrational levels, all with appreciable lifetimes. The $^1\Sigma_u^+$ state, which correlates with the $^2S+^2P$ asymptote, would be expected to have a bond order near zero. However, the wavefunction is dominated by Be^0+Be^{2+} in the region of the molecular well, and this produces four bound vibrational levels with appreciable lifetimes. The $^3\Pi_u$ state has two one-electron bonds, in analogy with the low-lying states of Al_2 (Bauschlicher *et al.* 1987). This bonding mechanism is also sufficiently strong to yield a substantial molecular well. However, the $^1\Pi_u$ state potential curve is purely repulsive, although it has a shoulder in the Franck–Condon region of the ground state.

Dications are most commonly detected by mass spectrometry. However, since Be has only one isotope in sufficient abundance with which to perform experiments, it would be difficult to detect Be_2^{2+} by this means, as it has the same charge-to-mass ratio as Be^+. Thus we have explored the possibility of detecting this cation spectroscopically. The transition moments are predicted to be large for both the $^1\Sigma_u^+$–X $^1\Sigma_g^+$ and $^1\Pi_u$–X $^1\Sigma_g^+$ band systems. The former band system, which should give rise to red-shifted bands in the ultraviolet, might provide a viable means of characterizing Be_2^{2+}. In addition, the latter transition might be used in an ion-pair coincidence experiment. Analogous calculations are being performed for the Mg_2^{2+} and Ca_2^{2+} dications, since these should be more amenable to experimental study.

$LaFe^{2+}$ was observed to have a very long lifetime in recent experiments (Huang and Freiser 1988). Considering the substantial difference between the IPs of La and Fe, it is not clear *a priori* to what extent the bonding can be described as either $La^{2+}Fe$ or La^+Fe^+. This is in contrast with the La^{2+}–hydrocarbon work described in the previous section, where both charges remain on the La, since the hydrocarbon IP is larger than the second IP of La (11·43 eV). Thus calculations can potentially give considerable insight into the nature of the bonding in these systems.

For $LaFe^{2+}$, we find (Bauschlicher and Langhoff 1989b) both a low-lying $^2\Delta$ and a $^4\Sigma^-$ state. The principal valence configurations of these states are given as

$$^2\Delta \quad [\mathrm{La}(5d\sigma)+\mathrm{Fe}(3d\sigma)]^2[\mathrm{La}(5d\pi)+\mathrm{Fe}(3d\pi)]^4\mathrm{Fe}(3d\delta^3),$$

$$^4\Sigma^- \quad [\mathrm{La}(5d\sigma)+\mathrm{Fe}(3d\sigma)]^2[\mathrm{La}(5d\pi)+\mathrm{Fe}(3d\pi)]^4\mathrm{Fe}(3d\delta^2 4s^1).$$

For both states there is a dσ bond and four electrons in the π orbital, three of which are contributed by Fe. Thus formally the bonding could be described as involving a single σ and π bond and a Fe lone pair. Although the bonds are highly polarized toward the Fe, this is compensated for by some back donation from the doubly occupied Fe 3dπ orbital. Thus the π bond has some double-bond character even though three of the electrons are derived from Fe. The populations given in table 13 show that the bonding involves a mixture of La^+ and La^{2+}. The contribution from La^{2+} occurs through polarization of the bond orbitals. The two states differ in the occupation of the non-bonding electrons. The $^2\Delta$ state is derived from the Fe^+ $3d^7$ state and has three non-bonding electrons in the 3dδ orbital, while the $^4\Sigma^-$ state is derived from the $3d^6 4s^1$ state and has two electrons in the 3dδ orbital and one in the 4s orbital. The 4s orbital is essentially non-bonding, since the different radial expectation values of the 3d and 4s orbitals prevents the formation of strong s and d bonds at the same r value. The 4s orbital mixes in 4p character, allowing it to polarize away from the La. Since the $^4\Sigma^-$ state is derived from the ground state of Fe^+ and retains more of the atomic exchange energy, it is the ground state by 1·28 eV at the MRCI level. However, both the $^4\Sigma^-$ and

Table 13. Valence population analysis for the natural orbitals of the MRCI wavefunction for the computed point closest to the minimum.

	$LaFe^{2+}$				$LaRu^{2+}$		YRu^{2+}	
	$^4\Sigma^-$		$^2\Delta$		$^2\Delta$		$^2\Delta$	
	La	Fe	La	Fe	La	Ru	Y	Ru
Net	1·56	0·44	1·40	0·60	1·54	0·46	1·16	0·84
s	0·22	1·15	0·16	0·42	−0·04	0·07	0·23	−0·08
p	0·05	0·16	0·07	0·22	−0·01	0·11	0·06	0·00
d	1·14	6·24	1·35	6·75	1·44	7·31	1·48	7·19

Table 14. Spectroscopic constants for selected transition-metal dications. The D_e value is computed as the difference in energy between the bottom of the molecular well and the top of the barrier.

	r_e molecular well (Å)	D_e molecular well (eV)	r barrier (Å)	Molecular well relative to asymptotes (eV)
		$LaFe^{2+}$ $^4\Sigma^-$		
CASSCF	3·38	0·61	5·49	1·70
MRCI	2·95	1·29	5·92	0·95
MRCI+Q	2·87	1·54	6·15	0·65
		$LaFe^{2+}$ $^2\Delta$		
CASSCF	2·85	0·54	4·04	2·37†
MRCI	2·76	1·42	4·42	1·32†
MRCI+Q	2·76	1·60	4·56	1·06†
		$LaRu^{2+}$ $^2\Delta$		
CASSCF	2·40	1·64	3·85	0·87
MRCI	2·35	2·03	5·25	0·14
MRCI+Q	2·36	2·18	5·33	−0·02
		YRu^{2+} $^2\Delta$		
CASSCF	2·39	1·05	3·81	1·78
MRCI	2·28	1·47	4·26	1·16
MRCI+Q	2·32	1·66	4·45	0·95

† Dissociates to Fe^+ $^4D(3d^64s^1)$.

the $^2\Delta$ states have large barriers to dissociation (table 14). The lowest vibrational level of the $^2\Delta$ state is computed to have a lifetime with respect to unimolecular decay of longer than 10^{600} s.

The ground state of $LaRu^{2+}$ is $^2\Delta$, since it is derived from the $4d^7$ ground state of Ru^+. Because the second-transition-row atoms form stronger bonds with their d orbitals than the first-transition-row atoms do, $LaRu^{2+}$ is even more stable than $LaFe^{2+}$ (see table 14). The MRCI and MRCI + Q potentials for the $^2\Delta$ state of $LaRu^{2+}$ are shown in figure 9. The potential has a very broad barrier to dissociation and a molecular well with a minimum near the energy of the lowest dissociation limit. As for $LaFe^{2+}$, the populations show a significant La^{2+} contribution to the bonding.

Since the first and second IPs of Y are larger than La, the relative importance of the Y^+Ru^+ and $Y^{2+}Ru$ contributions to the bonding are potentially different from the analogous molecules containing La. Although YRu^{2+} is strongly bound and has a barrier to dissociation that is comparable with $LaFe^{2+}$, the populations do indicate a much smaller charge contribution from Y^{2+} than from La^{2+}. The significant binding energy for these systems derives from the multiple bonding. It is likely that many other transition-metal diatomic dications will also be metastable with effectively infinite lifetimes.

4. Conclusions

We have illustrated the diversity of the bonding for transition-metal ions. In the case of electrostatic bonding the metal ions reduce repulsion by localizing the d holes,

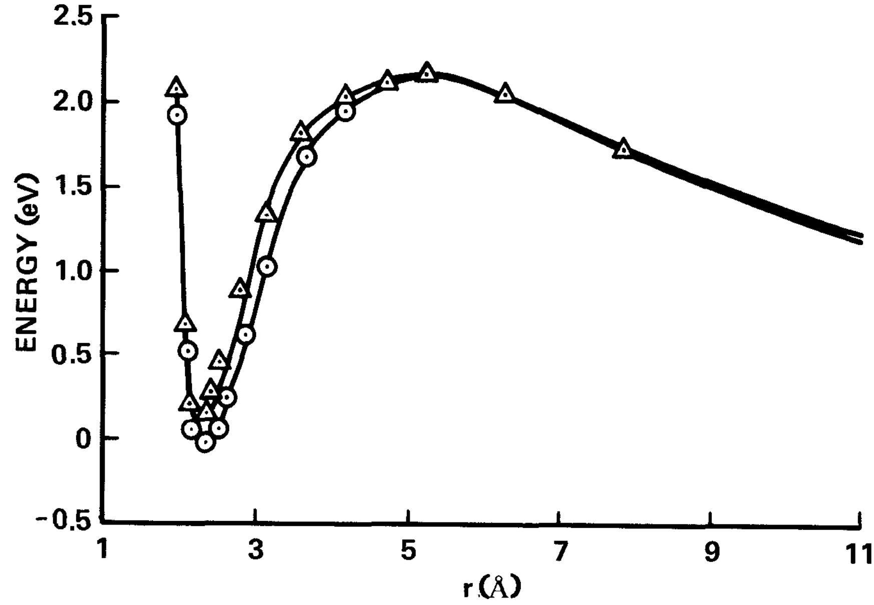

Figure 9. The MRCI (△) and MRCI + Q (○) potentials for the $^2\Delta$ state of $LaRu^{2+}$. The zero of energy is La^+ (^3F) + Ru^+ (^4F).

sp polarization, sd hybridization, s-to-d promotion and bending. In the case of dative bonding, such as in the transition-metal carbonyl ions, the d orbitals are occupied in such a manner to minimize the σ repulsion, but also to maximize the donation into the empty $2\pi^*$ orbitals. For covalent bonding, a strong mixing of asymptotes also occurs to allow the formation of the strongest bond. The interaction of La^+ and La^{2+} with hydrocarbons shows that the covalent interaction is much stronger than the electrostatic interaction. In many of the systems the monocations can still form multiple bonds or donate electrons to the other component. In all cases the relative importance of these effects depends greatly on the relative energies of the different ion asymptotes. When several ligands are present, the cost of promotion or hybridization can be shared, and therefore the balance of the different asymptotes altered. This can lead to a second-ligand binding energy that is larger than the first, something that cannot occur to the same extent for the simple metal ions. Caution is therefore required when extrapolating from simple metal ion studies to transition-metal ions.

Not only do the calculations give insight into interpreting the information obtained in experiment, but also they help us to understand the diversity of transition-metal bonding and to calibrate the methods. This will help to improve the quality of calculations on the neutral systems.

Acknowledgments

We would like to thank B. S. Freiser, P. B. Armentrout, R. R. Squires, P. J. Brucat and J. Michl for sending us results of their work prior to publication and for helpful discussions. In addition, a number of our colleagues at Ames Research Center, National Aeronautics and Space Administration have contributed to this work. We would especially like to thank L. A. Barnes, H. Partridge, L. G. M. Pettersson and M. Rosi.

References

Ahlrichs, R., Böhm, H. J., Brode, S., Tang, K. T., and Toennies, P. J., 1988, *J. chem. Phys.*, **88**, 6290.

Ahlrichs, R., Scharf, P., and Ehrhardt, C., 1984, *J. chem. Phys.*, **82**, 890.

Armentrout, P. B., and Georgiadis, R., 1988, *Polyhedron*, **7**, 1573.

Barnes, L. A., Rosi, M., and Bauschlicher, C. W., 1990, *J. chem. Phys.* (in the press).

Bauschlicher, C. W., Bagus, P. S., Nelin, C. J., and Roos, B. O., 1986, *J. chem. Phys.*, **85**, 354.

Bauschlicher, C. W., and Barnes, L. A., 1988, *Chem. Phys.*, **124**, 383.

Bauschlicher, C. W., and Langhoff, S. R., 1989a, *Chem. Phys. Lett.*, **158**, 409; 1989b, *Ibid.*, **161**, 383.

Bauschlicher, C. W., Langhoff, S. R., and Partridge, H., 1989a, *J. chem. Phys.*, **91**, 4733.

Bauschlicher, C. W., Langhoff, S. R., Partridge, H., and Barnes, L. A., 1989b, *J. chem. Phys.*, **91**, 2399.

Bauschlicher, C. W., Partridge, H., and Langhoff, S. R., 1990, *Chem. Phys. Lett.*, **65**, 272.

Bauschlicher, C. W., Partridge, H., Langhoff, S. R., Taylor, P. R., and Walch, S. P., 1987, *J. chem. Phys.*, **86**, 7007.

Bauschlicher, C. W., and Rosi, M., 1990, *Chem. Phys. Lett.*, **165**, 501.

Bauschlicher, C. W., and Walch, S. P., 1982, *J. chem. Phys.*, **76**, 4560.

Blomberg, M., Brandemark, U., Johansson, J., Siegbahn, P., and Wennerberg, J., 1988, *J. chem. Phys.*, **88**, 4324, and references therein.

Blomberg, M. R. A., Siegbahn, P. E. M., and Bäckvall, J.-E., 1987, *J. Am. chem. Soc.*, **109**, 4450.

Böttner, E., Dimpl, W. L., Ross, U., and Toennies, J. P., 1975, *Chem. Phys. Lett.*, **32**, 197.

Buckner, S. W., and Freiser, B. S., 1988, *Polyhedron*, **7**, 1583.

Cassady, D. S., and Freiser, B. S., 1984, *J. Am. chem. Soc.*, **106**, 6176.

Chong, D. P., and Langhoff, S. R., 1986, *J. chem. Phys.*, **84**, 5606.

Chong, D. P., Langhoff, S. R., Bauschlicher, C. W., Walch, S. P., and Partridge, H., 1986, *J. chem. Phys.*, **85**, 2850.

Cowan, R. D., and Griffin, D. C., 1976, *J. opt. Soc. Am.*, **66**, 1010.

Distefano, G., 1970, *J. Res. natn. Bur. Stand.*, **74**, 233.

Fischer, A. K., Cotton, F. A., and Wilkinson, G., 1957, *J. Am. chem. Soc.*, **79**, 2044.

Gdanitz, R. J., and Ahlrichs, R., 1988, *Chem. Phys. Lett.*, **143**, 413.

Gatland, I. R., 1981, *J. chem. Phys.*, **75**, 4162.

Halle, L. F., Crowe, W. E., Armentrout, P. B., and Beauchamp, J. L., 1984, *Organometallics*, **3**, 1694.

Hanratty, M. A., Beauchamp, J. L., Illies, A. J., Van Koppen, P., and Bowers, M. T., 1988, *J. Am. chem. Soc.*, **110**, 1.

Hay, P. J., and Wadt, W. R., 1985, *J. chem. Phys.*, **82**, 299.

Huang, Y., and Freiser, B. S., 1988, *J. Am. chem. Soc.*, **110**, 4435.

Kunze, K. L., and Harrison, J. F., 1989, *J. phys. Chem.*, **93**, 2983, and references therein.

Lamm, D. R., Thackston, M. G., Eisele, F. E., Ellis, H. W., Twist, J. R., Pope, W. M., Gatland, I. R., and McDaniel, E. W., 1981, *J. chem. Phys.*, **74**, 3042.

Langhoff, S. R., and Bauschlicher, C. W., 1988, *Ann. Rev. phys. Chem.*, **39**, 181.

Langhoff, S. R., Bauschlicher, C. W., Pettersson, L. G. M., and Partridge, H., 1987, *J. chem. Phys.*, **86**, 268.

Lessen, D., and Brucat, P. J., 1988, *Chem. Phys. Lett.*, **152**, 473; 1989a, *J. chem. Phys.*, **90**, 6296; 1989b, *Ibid.*, **91**, 4522.

Magnera, T. F., David, D. E., and Michl, J., 1989, *J. Am. chem. Soc.*, **111**, 4100.

Mandich, M. L., Halle, L. F., and Beauchamp, J. L., 1984, *J. Am. chem. Soc.*, **106**, 4403.

Marinelli, P. J., and Squires, R. R., 1989, *J. Am. chem. Soc.*, **111**, 4101.

Moore, C. E., 1949, *Atomic Energy Levels*, U.S. National Bureau of Standards Circular No. 467.

Olson, R. E., and Liu, B., 1979, *Chem. Phys. Lett.*, **62**, 242.

Pettersson, L. G. M., Bauschlicher, C. W., Langhoff, S. R., and Partridge, H., 1987, *J. chem. Phys.*, **87**, 481.

Polak-Dingels, P., Rajan, M. S., and Gilason, E. A., 1982, *J. chem. Phys.*, **77**, 3983.

Powers, T. R., and Cross, R. J., 1973, *J. chem. Phys.*, **58**, 626.

Rohlfing, C. M., Hay, P. J., and Martin, R. L., 1986, *J. chem. Phys.*, **85**, 1447.

Rosi, M., and Bauschlicher, C. W., 1989, *J. chem. Phys.*, **90**, 7264; 1990, *Chem. Phys. Lett.* **166**, 189.

ROSI, M., BAUSCHLICHER, C. W., LANGHOFF, S. R., and PARTRIDGE, H., 1990, *J. phys. Chem.* (submitted).

SCHAMP, H. W., and MASON, E. A., 1958, *Ann. Phys.* (*N.Y.*), **4**, 233.

SCHILLING, J. B., GODDARD, W. A., III, and BEAUCHAMP, J. L., 1987a, *J. Am. chem. Soc.*, **109**, 5565; 1987b, *J. phys. Chem.*, **91**, 4470.

SIEGBAHN, P. E. M., 1984, *Faraday Symp. chem. Soc.*, **19**, 97.

SKULLERUD, H. J., 1973, *J. Phys.* B, **6**, 918.

SMALLEY, R. E., 1985, *Comparison of* ab initio *Quantum Chemistry with Experiment for Small Molecules*, edited by R. J. Bartlett (Dordrecht: D. Reidel), p. 53.

SUNDERLIN, L. S., and ARMENTROUT, P. B., 1989, *J. Am. chem. Soc.*, **111**, 3845.

TAKEBE, M. J., 1983, *Chem. Phys.*, **78**, 7223.

WALCH, S. P., and BAUSCHLICHER, C. W., 1983, *J. chem. Phys.*, **78**, 4597.